Abstract: Synthetic chemical probes designed to simultaneously targeting multiple sites of protein surfaces are of interest owing to their potential application as site specific modulators of protein–protein interactions. A new approach toward bivalent inhibitors of mammalian type I geranylgeranyltransferase (GGTase I) based on module assembly for simultaneous recognition of both interior and exterior protein surfaces is reported. The inhibitors synthesized in this study consist of two modules linked by an alkyl spacer; one is the tetrapeptide CVIL module for binding to the interior protein surface (active pocket) and the other is a 3,4,5-alkoxy substituted benzoyl motif that contains three aminoalkyl groups designed to bind to the negatively charged protein exterior surface near the active site. The compounds were screened by two distinct enzyme inhibition assays based on fluorescence spectroscopy and incorporation of a [^{3}H]-labeled prenyl group onto a protein substrate. The bivalent inhibitors block GGTase I enzymatic activity with K_i values in the submicromolar range and are approximately one order of magnitude and more than 150 times more effective than the tetrapeptide CVIL and the methyl benzoate derivatives, respectively. The bivalent compounds **6** and **8** were shown to be competitive inhibitors, suggesting that the CVIL module anchors the whole molecule to the GGTase I active site and delivers the other module to the targeting protein surface. Thus, our module-assembly approach resulted in simultaneous multiple-site recognition, and as a consequence, synergetic inhibition of GGTase I activity, thereby providing a new approach in designing protein-surface-directed inhibitors for targeting protein–protein interactions.

Keywords: enzymes · GGTase I · inhibitors · proteins · proteomimetics

Introduction

Protein–protein interactions play a central role in numerous biological processes, including programmed cell death, proliferation and differentiation, and aging. In humans, roughly 40000 to 200000 protein interactions are estimated to exist.[1] Low-molecular-weight compounds that modulate such interactions in a selective manner are useful as probes to elucidate biological functions as well as drug leads for new therapeutic agents to target specific protein interfaces. Much effort has recently focused on the rational design of inhibitors based on proteomimetic strategies[2,3] to modulate protein–protein interactions, and a number of studies have been reported with success in this field.[4–6] For example, a general solution called "protein grafting" has been developed for transferring the functional epitope into a rigid miniature protein scaffold.[7,8] Similar approaches in combination with phase-display technique have also recently been developed with β-sheet templates[9,10] and β-hairpin cyclic peptidomimetics.[11]

Hamilton and co-workers used an elegant approach to create synthetic mimics of the antibody complementarity determining region (CDR) with nonpeptidic scaffolds, such as calixarenes[12,13] and porphyrins,[14–16] that accumulate multiple functional groups for targeting protein surfaces. These large synthetic antibody mimics were shown to require a large molecular surface for strong binding to the target. This approach demonstrated that the functionality of natural antibodies can be possibly mimicked by rationally designed synthetic molecules. However, in these examples, the molecular weight of the synthetic scaffold was still large. Increasing the binding affinity while decreasing the size of the molecule that is necessary for selective targeting is a challenging problem. To overcome this problem, we propose a strategy for protein-surface recognition that involves anchoring an exterior surface-binding module to an interior surface-binding module. The resulting bivalent compounds are expected to show increased affinity towards the target protein while leading to a decrease in the size of the protein-surface recognition scaffold required owing to a synergetic effect. One approach to test this hypothesis is the case of enzyme-inhibitor design in which a substrate mimic with high binding affinity and selectivity to the enzyme active site is linked to an exterior binding module that targets the appropriate sites on the protein surface. The resulting bivalent compounds are predicted to increase binding affinity (taking advantage of ΔG), and therefore the size of exterior binding module should decrease compared with that required for binding to the target by itself.

Strategies for bivalent or bisubstrate receptors have been utilized in recent chemical-biology studies, such as protein dimerization,[17,18] lead identification,[19] protein modifications,[20] and enzyme inhibitors.[21–30] Srivastava, Mallik, and co-workers have developed an efficient strategy to target the surface-exposed histidine side chains by using an imino-

[a] S. Machida, Prof. N. Kato, Prof. J. Ohkanda
The Institute of Scientific and Industrial Research (ISIR)
Osaka University, 8–1 Mihogaoka, Ibaraki, Osaka 567–0047 (Japan)
Fax: (+81) 6-6879-8474
E-mail: johkanda@sanken.osaka-u.ac.jp

[b] K. Usuba, A. Yano, Prof. K. Harada
Department of Life Sciences
Tokyo Gakugei University, Koganei, Tokyo 184–8501 (Japan)

[c] M. A. Blaskovich, Prof. S. M. Sebti
Drug Discovery Program at H. Lee Moffitt Cancer Center and Research Institute, Department of Molecular Medicine
University of South Florida, Tampa, FL 33612–9497 (USA)

Supporting information for this article is available on the WWW under http://www.chemeurj.org/ or from the author.

diacetate copper(II) complex.[24,31] In these examples, however, the motifs for the protein surface were designed for pinpoint binding of one or two amino acid side chains instead of targeting the large (≈1600 Å^2) surface areas that are typically involved in protein–protein interactions.[2-4] For modulating protein-surface functions, the anchoring strategy of a relatively large exterior binding motif with a smaller interior binding motif would provide a new approach for designing site-specific protein-surface receptors. As far as we are aware, there are no examples of nonpeptidic bivalent enzyme inhibitors that target the large protein surface areas that are involved in native protein–protein interactions.

Type I geranylgeranyltransferase (GGTase I)[32] is a heterodimeric zinc metalloenzyme and a member of the protein prenyltransferase family. This family of enzymes catalyzes the first step in a lipid post-translational modification that affects nearly 0.5% of cellular proteins.[33] Mammalian GGTase I is responsible for transferring a C20 geranylgeranyl group from geranylgeranyl pyrophosphate (GGPP) to a cysteine residue of the carboxy-terminus CAAX tetrapeptide of a target substrate protein; where C is cysteine, AA is an aliphatic dipeptide, and, in most cases, X is leucine or phenylalanine.[34] During the last decade, protein prenylation has become a major focus in anticancer research, and the major effort in developing prenyltransferase inhibitors focused on a related enzyme called farnesyltransferase (FTase). The aim was the specific inhibition of malignant transformation caused by mutated Ras and other farnesylated proteins.[35-37] The preclinical evaluation of FTase inhibitors was successful, with little toxicity, and several compounds are currently in clinical trials.[38]

Recently, GGTase I has been gaining much attention[39,40] owing to its potential to be a new target, not only for anticancer drugs,[41-45] but also for other diseases such as smooth muscle hyperplasia[46] and hepatitis C.[47] Its substrate proteins, such as RhoA,[48] RhoC,[49] Rac1,[50] Cdc42,[51] and RalA,[52] have been found to be implicated in promoting tumorigenesis and cancer metastasis. Very recently, a study using a GGTase I deficient mouse model has shown that GGTase I deficiency apparently improves the percentage of survival in mice with K-Ras-induced lung cancer, supporting the potential of GGTase I to be a clinical target.[44] A further significant observation that has been reported is that K-Ras4B, the most frequently mutated form of Ras in human tumors, becomes a substrate for GGTase I when FTase is blocked, and retains full biological activity.[53-55] As at least 5–10 times more proteins are geranylgeranylated than are farnesylated and the complex signaling pathways involving geranylgeranylated proteins have not been fully characterized, the development of potent and selective GGTase I inhibitors would provide useful tools for protein prenylation studies.

Mammalian GGTase I consists of a 48-kDa α subunit and a 43-kDa β subunit, which possesses the hydrophobic active pocket. The crystal structures of the ternary complex of GGTase I bound to the peptide and a GGPP analogue have revealed that there is a characteristic acidic region on the α-subunit protein surface near the entrance to the active pocket.[56-58] A number of studies have demonstrated that an unusual polylysine region near the carboxyl terminus of K-Ras4B is a critical determinant for geranylgeranylation catalyzed by GGTase I when FTase is inhibited.[59-62] Therefore, it is most likely that when the enzyme binds to K-Ras4B, the electrostatic attraction triggers the protein–protein interaction at the protein surface of GGTase I. In other words, GGTase I can be regarded as an enzyme that utilizes two distinct protein surfaces for substrate recognition in its native task, one is the interior surface of the substrate-binding cavity and the other is the protein exterior surface near the active site.

We therefore applied the concept of bivalent inhibitor design for simultaneous targeting of both surfaces of GGTase I (Figure 1). The interior surface-binding module

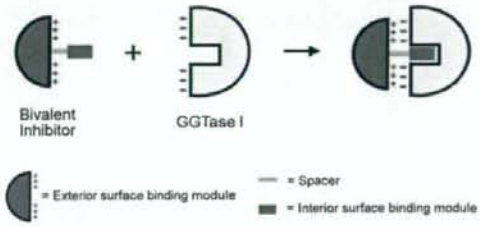

Figure 1. A schematic representation of the inhibitor design for simultaneous targeting of interior and exterior protein surfaces. Bivalent hybrid compound consist of an exterior surface-binding module (red) derived from a methyl gallate, an alkyl spacer (green), and an interior surface-binding module, Cys-Val-Ile-Leu-OH tetrapeptide.

(Figure 1, blue) should bind into the active pocket in a selective manner and should anchor the whole molecule near the pocket, whereas the exterior surface-binding module (Figure 1, red) requires relatively divergent structural features and multiple positively charged groups for the electrostatic interaction with the GGTase I surface. To explore the minimal and favorable distance in between the modules, we used different length spacers (Figure 1, green).

Herein, we describe the rational design of GGTase I bivalent inhibitors for simultaneous targeting of interior and exterior protein surfaces based on the module assembly strategy described in Figure 1.

Results and Discussion

Inhibitor design and chemistry: According to the GGTase I crystal structure, the substrate-binding pocket opens into the extensive α–β subunit interface and extends into the hydrophobic funnel-shaped cavity of the β subunit with an approximate inner diameter of 15 Å and a depth of 14 Å.[63] Near the entrance of the binding pocket, there is a characteristic cluster of acidic amino acid residues on the α-subunit protein surface where Glu125α, Glu160α, Glu161α, Glu187α, Asp191α, Glu229α, and Asp230α are located on

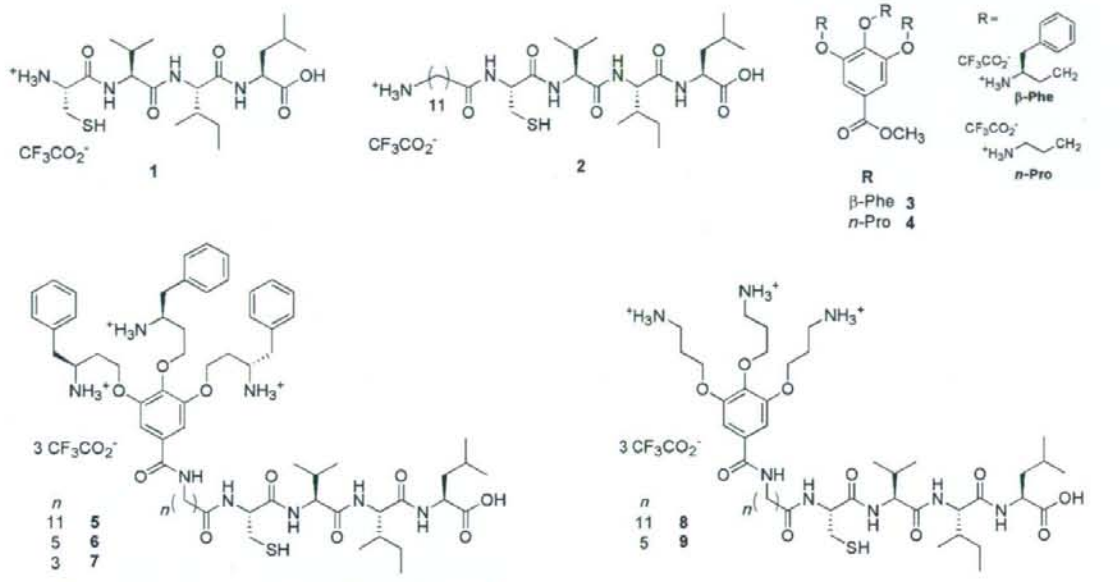

Scheme 1. Modules and hybridized compounds synthesized in this study.

the edge of the pocket lip. The compounds prepared on the basis of the design strategy are summarized in Scheme 1. For the interior surface binding module, Cys-Val-Ile-Leu-OH tetrapeptide (**1**), the CAAX sequence that is seen in GGTase I substrate proteins Rap-2b, and several others,[64] became our first choice because of its affinity to GGTase I with selectivity (IC_{50}/GGTase I = 2.3 μM; IC_{50}/FTase = 11 μM).[65] The size of the acidic surface of GGTase I is approximately 90 Å^2 and contains the seven acidic amino acid residues as well as several hydrophobic or neutral residues, such as Leu156α, Ala157α, Gln195α, and Asn194α. A molecular-modeling study showed that the methyl-3,4,5-trialkoxy-substituted benzoate derived from β-homophenylalanine derivative (**3**) possibly provides a complementary size (≈84 Å^2). In a further attempt to reduce the size of the exterior surface-binding module, *n*-propyl amine substituted derivative (**4**), in which three benzyl groups in **3** were removed, was also designed. These compounds were readily synthesized by alkylation of methyl gallate with the corresponding *N*-protected amino alkyl bromides, followed by deprotection (see the Supporting Information). These exterior surface-binding modules were attached to the N terminal of **1** by spacers of different lengths to give the bivalent hybrid compounds **5**–**9**.

To check whether the bivalent molecular sizes and shapes are relevant for the simultaneous two-site recognition, a superimposed model structure of **5** and GGTase I was built based on the previously reported X-ray crystal structure of the ternary complex of GGTase I[58] bound to a GGPP analogue and KKKSKTKCVIL. Within the complex, the portion of KKKSKTK was removed and the structure of **5** without the CVIL moiety was installed. The resulting model showed that the trisubstituted benzoyl part provides an appropriate shape to bind the targeted acidic region of GGTase I (Figure 2).

Figure 2. A superimposed model of **5** (yellow, CPK) and GGTase I crystal structure (PDB: 1N4Q). The catalytic Zn ion (green, CPK), GGPP analogue (stick); The bright area (right) and shadowed portions are the α and β subunits, respectively. Negatively charged and positively charged surfaces are shown in red and blue, respectively. DS Viewer 6.0.

Initial screening for inhibition activity by fluorescent enzyme assay: To examine whether the module-assembly approach results in bivalent inhibitors with better potency towards GGTase I, the compounds were initially screened at 5 μM for their ability to inhibit GGTase I in a fluorescent assay[66] by using geranylgeranyl pyrophosphate (GGPP; 5.0 μM) and the environmentally sensitive fluorogenic substrate, N-dansyl-Gly-Cys-Val-Ile-Leu-OH (DansGCVIL; 1.0 μM, $K_m = (0.28 \pm 0.04)$ μM; dansyl = 5-(dimethylamino)-naphthalene-1-sulfonyl; see Scheme S21 in the Supporting Information) in Tris-HCl buffer solution (Tris = tris(hydroxymethyl)aminomethane). This substrate increases the fluorescent intensity upon geranylgeranylation at the cysteine thiol group. Recombinant mammalian GGTase I was expressed and purified by a method previously reported.[67] The fluorescent increase was monitored for 5 min and the percentage of inhibition was calculated by comparison with the standard slope, which was taken from the reaction in the absence of inhibitors (see the inset in Figure 3A). The percentage of inhibition of GGTase I at a compound concentration of 5 μM is shown in Figure 3A. As expected, the various modules of the bivalent compounds were weak GGTase I inhibitors on their own. For example, CVIL (**1**), which has been shown to be a competitive inhibitor for GGTase I,[65] inhibited 42% of the enzyme activity (see the inset of Figure 3A); and compounds **2**–**4** inhibited the enzyme by 2–26%. However, the bivalent compound **6**, in which the modules **1** and **3** were hybridized, and compound **8**, in which modules **1** and **4** were linked, were both found to be more effective than either module alone and showed more than 87% inhibition. Concentration–response studies showed that the compound **6** inhibition curve is sigmoidal with an IC_{50} value of 1.0 μM and a K_i of (0.22 ± 0.04) μM, both of which were calculated by using the Cheng–Prusoff equation (Figure 3B).[68] In contrast, the curves for the modules **1**, **2**, and **3** were apparently shifted to the higher concentration region. For example, the concentration required for 50% inhibition in the case of the tetrapeptide CVIL (**1**) was 6.9 μM, which was approximately seven times higher than that of **6**.

Concentration–response curves of the bivalent compounds (**5**–**7**) containing spacers of different lengths are summarized in Figure 4A. The results show that the spacer length affects the inhibitory activity of the bivalent compounds. Compound **7** ($n=3$), which consists of a shorter spacer for the C2 unit than **6** ($n=5$), was slightly less active than **6** ($K_i = (0.48 \pm 0.11)$ μM). On the other hand, compound **5** ($n=11$), with a spacer length twice as long as that of **6** was less potent. This suggests that for compounds with the β-homophenylalanine type module, the longer spacers diminish the binding affinity to GGTase I owing to the entropical disadvantage.[69] However, as shown in Figure 4B, compound **8**, which has an equal length of spacer to that of **5** and a much simpler exterior module, restores the activity with a K_i value of (0.42 ± 0.09) μM. Elimination of the three benzyl groups from the exterior binding module in **5** should result in increased flexibility as well as decreased hydrophobicity around the three amino side chains of the benzoyl moiety in

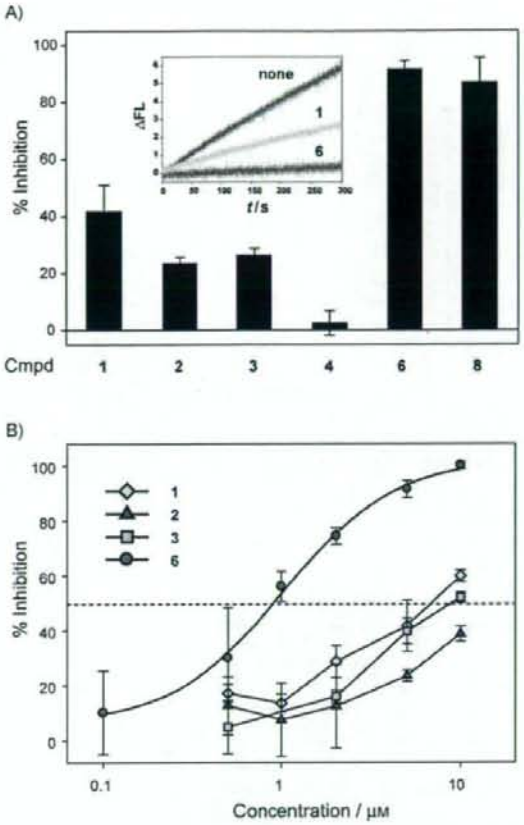

Figure 3. Fluorescent GGTase I inhibition assays were carried out by using GGPP (5 μM) and the fluorogenic substrate, DansGCVIL (1 μM) in 50 mM Tris-HCl, pH 7.5 at 30°C. A) The results of primary screening of the % inhibition of GGTase I in the presence of 5 μM of module compounds (**1**–**4**) and the bivalent compounds (**6** and **8**). Inset: the time course fluorescence change at 520 nm (ex: 340 nm) in the absence of (blue) or in the presence of 5 μM of inhibitors (**1**, blue; **6**, red). The slopes were used for the calculations of percentage of inhibition. B) Concentration–response curves of the modules (**1**, **2**, and **3**) and the corresponding hybridized compound **6** plotted the % inhibition against the inhibitor concentrations. The IC_{50} values were then used to calculate the inhibitory constants, K_i, by the Cheng–Prusoff equation (see reference [68]). The standard deviation is given for $n=3$. δI_f = change in fluorescence intensity.

8 (calculated log P values: −0.9 for **3**, 5.08 for **4**).[70] Therefore, a possible explanation for the significant difference in the activity might be 1) with the long spacer ($n=11$), the three 1-amino-1-benzyl-propyloxy groups in **5** do not take a suitable conformation for binding to the targeted surface owing to rigidity, whereas 1-amino-propyloxy groups are more flexible, thus the spacer length ($n=11$) was able to deliver the moiety to the targeted site; or 2) the high hydrophobicity of **5** might result in random binding or possible aggregation. This observation prompted us to synthesize compound **9** in which the better aminopropyl module and the

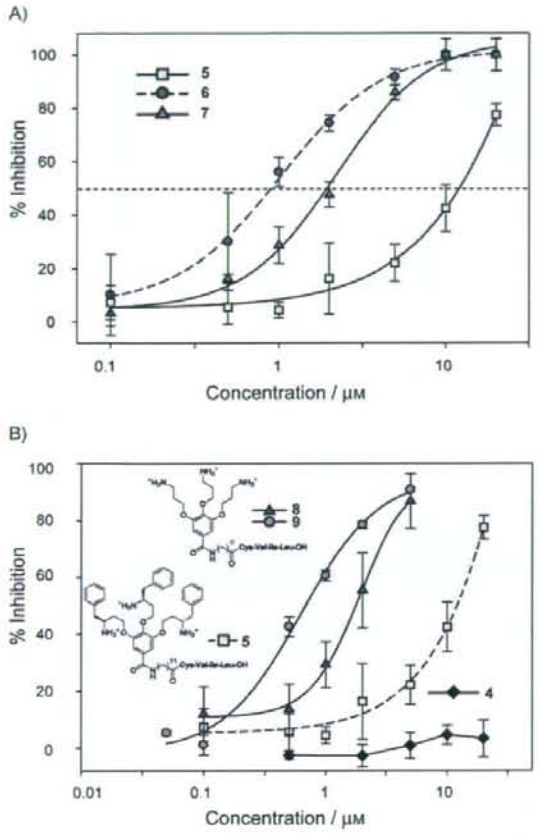

Figure 4. A) Dose–response curves for A) the bivalent compounds (**5**, **7**) with different a different spacer length than **6** and B) the methyl gallate derivative (**4**) compared with bivalent compound **8** and **9**, which consist of the methyl gallate as the exterior surface-binding module. The data set for **6** (A) and **5** (B) are shown for comparison (dashed line). The standard deviation values are given for $n=3$.

optimal length of spacer ($n=5$) were combined. As shown in Figure 4B, **9** indeed showed improved activity compared with **8** with an IC_{50} value of 0.62 μM and a K_i of (0.14 ± 0.03) μM, which has a similar activity to **6** and with a reduced molecular weight of 270. This suggests that the molecular size can be tuned by choosing 1) the minimal critical functional groups for the exterior binding module and 2) the most appropriate spacer length for the combination of modules. Notably, compound **4** showed no apparent inhibitory activity by itself (Figure 4B). The weak activity of modules **1** and **4**, and the synergistic effect seen with the bivalent inhibitor **9**, validates our module assembly approach that targets two critical sites on GGTase I.

Selectivity in GGTase I inhibition: To confirm the observation seen in the fluorescent assay and to evaluate the selectivity of our bivalent inhibitor for GGTase I over the related enzyme, FTase, we further tested the compounds (**1–8**) by a more widely used method, which measures the incorporation of [^{3}H]GGPP and [^{3}H]FPP (farnesylpyrophosphate) into the protein substrates, H-Ras-CVLL and H-Ras-CVLS, respectively, by using previously described methods.[71] The moderate inhibition activities against GGTase I of the tetrapeptides **1** and **2** were confirmed as shown in Table 1. No inhibition activity against FTase was detected with **1** or **2**, which is in agreement with the fact that CVIL is a selective inhibitor for GGTase I over FTase.[65] Neither benzoate derivative **3** nor **4** showed any activity. All the bivalent compounds (**5–8**) were confirmed to be potent for GGTase I with IC_{50} values in the submicromolar range (Table 1) and most importantly, no inhibition was detected against FTase (IC_{50}: GGTase I/FTase > 167 in the case of **8**). The selectivity observed here clearly indicates that the CVIL module in each bivalent compound recognizes and binds to the GGTase I active pocket but not to the FTase pocket. These results demonstrate that specificity is not compromised by our design strategy.

Table 1. IC_{50} values for inhibition of GGTase I and FTase in vitro by modules (**1–4**) and bivalent inhibitors (**5–8**).

Cmpd	IC_{50} [μM][a] GGTase I	FTase
1	4.8 ± 1.7	> 100
2	1.4 ± 0.5	> 100
3	> 100	> 100
4	> 100	> 100
5	0.98 ± 0.45	> 100
6	0.64 ± 0.06	> 100
7	0.66 ± 0.05	> 100
8	0.60 ± 0.03	> 100

[a] Where the standard deviation is given for $n=3$, or $n=1$.

The spacer-length effect was also observed in this assay, showing that compounds **6** and **7** ($n=5$ and 3, respectively) were more potent ($IC_{50}=0.64$ and 0.66 μM, respectively) than compound **5** ($n=11$, $IC_{50}=0.98$ μM). It is noteworthy that compound **8**, a with smaller and less hydrophobic exterior binding module than **6**, was found to be equally effective with an IC_{50} value of 0.60 μM, which was an improvement of eight times and greater than 167 times those of the corresponding modules, **1** and **4**, respectively. Again, these results confirmed that the molecular size of the hybrid inhibitors can be optimized by appropriately combining the modules.

Mode of inhibition: We next wanted to confirm that the inhibition mode of the bivalent inhibitor and the CVIL tetrapeptide was identical. To this end, Lineweaver–Burk analysis was carried out for peptide **1** and the bivalent compounds **6** and **8**. The data were analyzed by using equations for competitive, noncompetitive, and uncompetitive inhibition models. The data set for **1** clearly fit the competitive model (Figure 5A; $K_i=(0.97\pm0.19)$ μM). As shown in Figure 5B for **6**, these data also showed the best fit to the competitive model with an intersection point on the y axis ($K_i=$

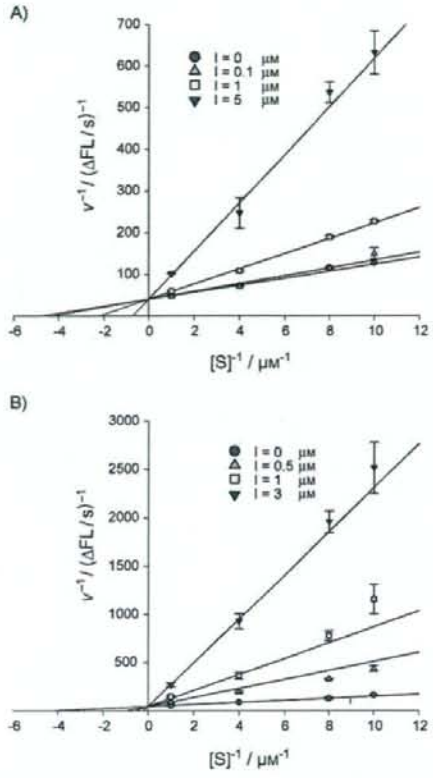

Figure 5. Kinetic analysis of the inhibition of GGTase I by CVIL tetrapeptide **1** and bivalent inhibitor **6**. GGTase I was treated with varying concentrations of A) the tetrapeptide **1** (0.1, 1, and 5 μM) and B) the bivalent compound **6** (0.5, 1, and 3 μM) with the substrate concentration increasing from 0.1 to 1 μM. [GGPP] = 5 μM, T = 293 K.

(0.15 ± 0.01) μM for **6** and (0.21 ± 0.03) μM for **8**; see Figure S2 in the Supporting Information for **8**).

As we used the native substrate peptide sequence for the interior surface binder, we wanted to clarify whether geranylgeranylation occurred on the thiol group of the bivalent compounds. The HPLC analysis showed that in the absence of inhibitor, the conversion of DansGCVIL to DansGC(GG)VIL was completed within 5 minutes (see Figure S3A in the Supporting Information), whereas under the same conditions but in the presence of 20 μM **6**, the geranylgeranylation of DansGCVIL was completely suppressed (see Figure S3B in the Supporting Information). Moreover, no change in the peak area of **6** nor new-product peak generation was detected for up to 50 minutes incubation with **6**, indicating that geranylgeranylation did not occur on the thiol group of **6** (see Figure S3C in the Supporting Information). This is consistent with previous work with FTase in which some CAAX tetrapeptide mimetic inhibitors are not farnesylated. The crystal structural study has revealed that these FTase inhibitors bind in a distinct conformation from the substrate,[72] suggesting that the conformation in the active-site-bound form is essential to dictate whether S-farnesylation occurs. Assuming that this is also the case in GGTase I, which is likely owing to its functional similarity, the binding of the exterior module to the protein surface may trigger structural changes of the interior binding module CVIL to avoid S-geranylgeranylation.

Conclusion

We have developed a new series of bivalent inhibitors for GGTase I based on a module assembly strategy for simultaneous targeting of interior and exterior protein surfaces. Coupling of CVIL tetrapeptide and a 3,4,5-trisubstituted benzoate derivative provided compounds **6** and **8** (K_i = 0.15 and 0.21 μM, respectively) and improved the inhibitory ability by approximately one order of magnitude and more than 150-fold compared with the corresponding modules. An explanation for the moderate additivity effect observed with the bivalent compounds compared with tetrapeptide **1** might be due to the remarkably weak affinity of the exterior binding modules **3** and **4**. All bivalent compounds were found to be highly selective for GGTase I over FTase (> 167 times). The spacer length was found to affect the potency, and very long spacers (n = 11) diminished the activity as seen in the case of **5**, which is consistent with a previous report.[69] Simply changing the exterior binder in **5** to one with less hydrophobic and more flexible side chains restored the activity, as seen in **8**. Thus, bivalent inhibitors targeting the exterior and the interior surfaces can be minimized by choosing the most appropriate modules and the spacer lengths. Interestingly, geranylgeranylation was not detected, at least in the case of **6**, suggesting that the exterior surface binding module may alter the CVIL conformation in the active pocket. Although it remains moderate, the synergetic inhibitory activity observed in this study strongly suggests that the exterior binding modules were specifically delivered to the targeted protein surface. Thus, we believe that the module-assembly strategy for designing bivalent protein inhibitors described herein provides a general strategy for specific targeting of the protein surface, which can be extended to other enzyme families for increased selectivity or for modulating protein–protein interactions.

We are currently extending this strategy to isozyme selective inhibitors and to dual inhibitors targeting characteristically distinct and identical protein-surface structures.

Experimental Section

Materials and instruments: Reagents and solvents were obtained from commercial sources without further purification unless otherwise noted. For the fluorescent enzyme assay, RF-5300PC equipped with a SA-100 temperature controller (Sansyo) was used. HPLC data were obtained from PU-2086 and a UV-2075 detector (JASCO) with Inertsil (C18-reverse phase column) column (GL Science). ^{1}H and ^{13}C NMR spectra were recorded on a JEOL JNM-LA 400 spectrometer. Low- and high-resolution mass spectra were collected by a JEOL JMS-T100 LC mass

spectrometer. Elemental analyses were performed on 2400CHN (Perkin Elmer).

Synthesis of 3,4,5-tris(3-amino-4-phenyl-1-butoxy)benzoic acid methyl ester trifluoroacetate (3): A solution of methyl gallate (101 mg, 0.549 mmol), [(1*S*)-3-bromo-1-(phenylmethyl)propyl]carbamic acid *tert*-butyl ester (**31**; 700 mg, 2.15 mmol; see the Supporting Information), potassium carbonate (444 mg, 3.21 mmol) in *N,N*-dimethylformamide (DMF; 20 mL) was stirred at 40 °C for 24 h. After removal of DMF, the product was extracted with 10% $CHCl_3$ in AcOEt (600 mL) and 10% citric acid, and the organic layer was dried over Na_2SO_4. The crude product was purified by SiO_2 column chromatography (gradient from $CHCl_3$ alone, to $CHCl_3$:AcOEt = 1:1, and then to $CHCl_3$:MeOH = 50:1) to give 3,4,5-tris(3-*N*-(*tert*-butoxy)amino-4-phenyl-1-butoxy)benzoic acid methyl ester (**32**; see the Supporting Information) as a white solid (464 mg, 91%). m.p.: 167–168 °C; ^{1}H NMR (400 MHz, $CDCl_3$): δ = 1.38 (m, 27H, Boc × 3 (Boc = *tert*-butyloxycarbonyl), 1.82–2.10 (m, 6H, 3-, 4-, and 5-OCH_2CH_2), 2.77–2.87 (m, 6H, 3,4, 5-CH_2Ph), 3.88 (s, 3H, -OCH_3), 4.07–4.12 (m, 9H, 3,4,5-OCH_2CH_2CH), 4.69 (br s, 2H, 3- and 5-NH), 5.28 (br s, 1H, 4-NH) and 7.17–7.28 ppm (m, 17H, aryl H); HRMS–FAB (*m/z*): [M^++H] calcd for $C_{53}H_{72}N_3O_{11}$, 926.5167; found, 926.5152. Trifluoroacetic acid (TFA; 500 μL) in CH_2Cl_2 (500 μL) was added to a solution of **32** (25 mg, 27.0 μmol) and the mixture was stirred at 0 °C for 1 h. After evaporation, Et_2O was added to the residue and the resulting white precipitate was collected by centrifugation to give compound **3** (30 mg, 100%). HPLC purity, 99%; ^{1}H NMR (400 MHz, $CDCl_3$): δ = 2.11–2.15 (m, 6H), 2.86 (m, 3H), 3.18 (m, 3H), 3.67 (m, 3H), 3.88 (s, 3H, OCH_3), 3.95 (s, 1H), 4.10 (s, 1H), 4.20 (s, 2H), 4.34 (s, 2H), 7.15–7.34 (m, 17H), 8.07–8.15 ppm (br s, 9H, NH_3); HRMS–FAB (*m/z*): [M^++H] calcd for $C_{38}H_{48}N_3O_5$, 626.3594; found, 626.3605.

Synthesis of *N*-[6-(3,4,5-tris(3-amino-4-phenyl-1-butoxy)benzolyamino)-hexylcarbonyl]-L-cisteinyl-L-valyl-L-isoleucyl-L-leucine trifluoroacetate (6): 1M KOH (1.3 mL, 1.3 mmol) was added to a solution of **32** (43 mg, 46.4 μmol) in CH_2Cl_2 (4 mL) and MeOH (8 mL) and the mixture was refluxed for 15.5 h. Evaporation, extraction with $CHCl_3$ (60 mL × 3) and 10% citric acid (25 mL), and concentration gave the corresponding carboxylic acid (**33**, see the Supporting Information) as a white solid (43 mg, 100%). m.p.: 141–144 °C; ^{1}H NMR (400 MHz, $CDCl_3$): δ = 1.38 (m, 27H, Boc × 3), 1.82–2.05 (m, 6H, 3-, 4-, and 5-OCH_2CH_2), 2.80–2.87 (m, 6H, 3-, 4-, and 5-CH_2Ph), 4.09–4.13 (m, 9H, 3-, 4-, and 5-OCH_2CH_2CH), 4.69 (br s, 2H, 3 and 5-NH), 5.28 (br, 1H, 4-NH) and 7.17–7.28 ppm (m, 17H, aryl H); HRMS–FAB (*m/z*): [M^++H] calcd for $C_{52}H_7N_3O_{11}$, 912.5010; found, 912.4990. Benzotriazol-1-yloxytris(pyrrolidino)phosphonium hexafluorophosphate (PyBop; 67 mg, 0.13 mmol) in CH_2Cl_2 (1 mL)was added to a solution of **33** (90 mg, 98.7 μmol), 6-aminohexanoic acid methyl ester hydrochloride (19 mg, 0.10 mmol), *N*-hydroxy-benzotriazole (HOBt; 31 mg, 0.20 mmol), and *N,N*-diisopropylethylamine (DIEA; 34 μL, 0.20 mmol) in DMF (5 mL) at 0 °C and the mixture was stirred at RT for 13 h. After concentration, the product was extracted with $CHCl_3$ (200 mL), 10% citric acid, 5% $NaHCO_3$, and brine. The crude product was purified by SiO_2 column chromatography ($CHCl_3$/MeOH = 20:1) to afford the desired product (**35**; see the Supporting Information) as a white solid (101 mg, 98%). m.p.: 190–195 °C; ^{1}H NMR (400 MHz, [D_6]DMSO): δ = 1.13–1.29 (m, 29H, 3-, 4-, and 5-Boc and -$CH_2CH_2CH_2CO_2CH_3$), 1.45–1.58 (m, 10H, -$CH_2CH_2CO_2CH_3$, -$CONHCH_2CH_2$ and 3-, 4-, 5-OCH_2CH_2), 1.77–1.90 (m, 6H, -OCH_2CH_2), 2.29 (t, J = 7.3 Hz, 2H, -$CH_2CO_2CH_3$), 2.66–2.78 (m, 6H, 3,4,5-CH_2Ph), 3.18–3.23 (m, 2H, -$CONHCH_2$), 3.56 (s, 3H, -CO_2CH_3), 3.83–3.99 (m, 9H, 3-, 4-, and 5-OCH_2CH_2CH), 6.55 (d, J = 8.3 Hz 1H, 4-N*H*Boc), 5.30 (d, J = 8.4 Hz, 2H, 3 and 5-N*H*Boc), 7.08 (s, 2H, benzoyl) 7.16–7.25 (m, 15H, 3-, 4-, and 5-Ph) and 8.33 ppm (m, 1H, NH); LRMS (ESI) [M^++Na] calcd for $C_{85}H_{82}N_4O_{12}$Na, 1061; found, 1061; elemental analysis calcd (%) for $C_{59}H_{82}N_4O_{12}$: C 68.18, H 7.95, N 5.39; found: C 67.99, H 7.90, N 5.30.

Compound **35** (85 mg, 82 μmol) was hydrolyzed in a similar manner as described above by using KOH to give the corresponding carboxylic acid **38** (see the Supporting Information) as a pale yellow amorphous solid (87 mg, 100%). m.p.: 168–172 °C; ^{1}H NMR (400 MHz, [D_6]DMSO): δ = 1.14–1.30 (s, 29H, 3-, 4-, and 5-Boc and $CH_2CH_2CH_2CO_2CH_3$), 1.46–1.55 (m, 4H, -$CH_2CH_2CO_2CH_3$ and -$CONHCH_2CH_2$), 1.76–1.91 (m, 6H, 3-, 4-, and 5-OCH_2CH_2), 2.20 (t, J = 7.1 Hz, 2H, -$CH_2CO_2CH_3$), 2.67–2.73 (m, 6H, 3-, 4-, and 5-$PhCH_2$), 3.18–3.23 (m, 2H, -$CONHCH_2$), 3.84–3.99 (m, 9H, 3-, 4-, 5-OCH_2CH_2CH), 6.59 (d, J = 8.8 Hz, 1H, 4-NHBoc), 6.81 (d, J = 8.5 Hz, 1H, 3- and 5-N*H*Boc), 7.09–7.26 (m, 17H, 3,4,5-Ph and benzoyl) and 8.34 (m, 1H, benzoyl-CONH) and 11.9 ppm (br s, 1H, -CO_2H); HRMS-FAB (*m/z*): [M^++H] calcd for $C_{58}H_{81}N_4O_{12}$ [M^++H]: 1025.5851; found: 1025.5835.

PyBop (50 mg, 96 μmol) in CH_2Cl_2 (1 mL) was added to a solution of the free acid **38** (72 mg, 70 μmol), H-Cys(Trt)-Val-Ile-Leu-O*t*Bu (Trt = trityl; 66 mg, 89 μmol), HOBt (25 mg, 0.16 mmol), and DIEA (25 μL, 015 mmol) in DMF (6 mL) at 0 °C. After stirring at room temperature for 17 h, concentration, extraction with $CHCl_3$, and purification by size-exclusion column chromatography (Sephadex LH-20, $CHCl_3$/MeOH = 1:1) gave the fully protected product (**41**; see the Supporting Information) as a white solid (86 mg, 70%). m.p.: 179–181 °C; ^{1}H NMR (400 MHz, $CDCl_3$): δ = 0.68–0.86 (m, 18H, γ-CH_3 Val, γ-CH_3 Ile, δ-CH_3 Ile, and 2δ-CH_3 Leu), 0.97–1.04 (m, 1H, γ-CH Leu), 1.13–1.86 (m, 54H, γ-CH_2 Ile and β-CH_2 Leu, β-CH Ile, β-CH Val, 3-, 4-, and 5-OCH_2CH_2, -$CONHCH_2(CH_2)_3$, O*t*Bu and 3-, 4-, 5-Boc), 2.08 (m, 2H, β-CH_2, Cys), 2.33 (m, 2H, -CH_2CONH), 2.67–2.73 (m, 6H, 3-, 4-, and 5-CH_2Ph), 3.17 (m, 2H, -$CONHCH_2$), 3.84–3.98 (m, 9H, 3-, 4-, and 5-OCH_2CH_2CH), 4.12–4.27 (m, 4H, α-CH Cys, Val, Ieu, and Leu), 6.55 (d, J = 8.4 Hz, 4-NHBoc), 6.78 (d, J = 8.8 Hz, 2H, 3- and 5-NHBoc), 7.09–7.33 (m, 32H, aryl-H), 7.50 (d, J = 8.9 Hz, 1H, NH), 7.88 (d, J = 8.8 Hz, 1H, NH), 8.09 (d, J = 8.3 Hz, 1H, NH) 8.16 (d, J = 7.9 Hz, 1H, NH), 8.31 ppm (m, 1H, CONH); elemental analysis calcd (%) $C_{101}H_{136}N_8O_{16}S \cdot 1.0H_2O$: C 68.52, H 7.97, N 6.33; found: C 68.57, H 7.87, N 6.22; HRMS–FAB (*m/z*): [M^++H] calcd for $C_{101}H_{139}N_8O_{16}S_1$, 1752.003; found, 1752.0000.

This compound was deprotected by treatment with 50% TFA in CH_2Cl_2 in the presence of 5% triethylsilane at 0 °C for 1 h. After concentration, the residue was suspended in Et_2O, sonicated, and centrifuged to collect the resulting white solid, which was washed with Et_2O several times, and dried to give **6**, a colorless white powder (21 mg, 100%). m.p.: 154–162 °C; ^{1}H NMR (400 MHz, $CDCl_3$): δ = 0.78–0.86 (m, 18H, 2γ-CH_3 Val, γ-, δ-CH_3 Ile, and 2δ-CH_3 Leu), 1.02–1.11 (m, 1H, γ-CH Leu), 1.24–1.96 (m, 18H, 3,4,5-OCH_2CH_2, -$CONHCH_2(CH_2)_3$, β-CH Val, β-CH and γ-CH_2 Ile, and β-CH_2 Leu), 2.13–2.18 (m, 2H, -CH_2CONH), 2.62–2.78 (m, 2H, β-CH_2 Cys), 2.83–2.97 (m, 6H, 3,4,5-$PhCH_2$), 3.90–3.93 (m, 2H, α-CH × 2), 4.09–4.20 (m, 7H, 3-, 4-, and 5-OCH_2 and α-CH), 4.40–4.45 (m, 1H, α-CH), 7.19–7.34 (m, 17H, 3-, 4-, and 5-Ph and benzoyl), 7.79–7.86 (m, 2H, -N*H*CH), 8.06–8.14 (m, 2H, -N*H*CH), 8.36–8.39 ppm (m, 1H, PhCONH); HRMS–FAB (*m/z*): [M^++H] calcd for $C_{60}H_{104}N_8O_{10}S_1$, 1153.6735; found, 1153.6702.

Protein expression and purification: The plasmids, GGTase I α subunit in pAlter-Ex2 (pAlter-Ex2-GGTα) and β subunit in pET28a (pET28a-GGTβ) were kindly provided by Prof. Casey from Duke University. The protein was expressed and purified as previously reported.[42,67] Briefly, the plasmids were successively transformed into BL21 (DE3) *E. coli* cells (Novagen), which grew until the optical density reached 0.6. GGTase I expression was induced by the addition of isopropyl-β-D-thiogalactoside (0.4 mM) and $ZnSO_4$ (0.5 mM), and the cells were harvested after 4 h and lysed. The soluble fraction of the cell lysate was bound to nickel agarose resin (Qiagen) by incubation for 1 h at 4 °C in a buffer solution containing Tris-HCl (20 mM, pH 7.7), NaCl (300 mM), imidazole (5 mM), dithiothreitol (DTT; 1 mM), and protease inhibitor mix. The proteins were eluted with increasing concentrations of imidazole, and the appropriate fractions were immediately dialyzed and concentrated. The purity of the protein solution was checked by SDS-PAGE gels (> 90%).

General conditions for fluorescent enzyme assay: The inhibition activities of the synthetic compounds against GGTase I were measured by a kinetic assay by using the fluorogenic substrate, dansyl-Gly-Cys-Val-Ile-Leu (DansGCVIL), which was prepared by solid-phase peptide synthesis (see Figures S21 and S22 in the Supporting Information). The peptide buffer solution (53 mM Tris-HCl, pH 7.5, 0.1 mM ethylenediaminetetraacetate (EDTA), 0.020% *n*-dodecyl-β-D-maltoside, 5.0 mM DTT) was used for preparation of DansGCVIL stock solution, and the assay buffer solution (50 mM Tris-HCl, pH 7.50, 1.2 mM $MgCl_2$, 1.2 μM $ZnCl_2$, 0.023% *n*-dode-

cyl-β-D-maltoside, 5 mM DTT) was used for enzyme dilution and for running the kinetic assay. Commercially purchased GGPP ammonium salt methanol solution from Sigma–Aldrich was diluted with 25 mM NH_4HCO_3 to 500 mM and stored at −80 °C in aliquots and further diluted to 110 μM before use (methanol content less than 5%). The peptide substrate, DansGCVIL, was dissolved in the peptide buffer solution (approximately 500 μM), and the concentration was determined from a standard curve of A_{340} versus the concentration of dansylglycine in the same buffer solution. Inhibitors were first dissolved in DMSO solution (1 or 30 mM) and further diluted with peptide buffer solution to various concentrations (1.1 μM to 2.2 mM), which were then used for the assay. The GGTase I solution (125 μM) was freshly diluted with the assay buffer solution prior to use (685 nM). The assays were performed at 30 °C by using a thermostated curvette holder. Solutions of DansGCVIL (10 μL), GGPP (10 μL), and inhibitor (10 μL) were added to the assay buffer solution (180 μL) in a 500-μL tube, which was incubated in a 30 °C water bath for 5 min. The GGTase I solution (10 μL) was added to this solution; the mixture was vortexed, quickly transferred to the cuvette, and the fluorescent intensity change at 520 nm (ex: 340 nm) was monitored for 5 min. The final concentrations of each component were: [DansGCVIL] = 1 μM, [GGPP] = 5 μM, [GGTase I] = 31 nM, [Inhibitors] = 0–100 μM (the content of DMSO in the final solution was less than 2%). The experiments for each concentration of inhibitor were repeated at least three times.

The raw data points were fit linearly and the resulting slopes were used to calculate IC_{50} values, which were determined by plotting the data as percent inhibition versus the log of the concentration of the inhibitors used. The data were fit to the sigmoidal Equation (1) by using SigmaPlot (version 10, Systat software, Inc.).

$$y = a + \frac{(b-a)}{1 + 10^{(c-x)d}} \quad (1)$$

In Equation (1), a and b are the minimal and maximal values of percentage of inhibition, x is the logarithm of the inhibitor concentration, c is the IC_{50} value, and d is the Hill slope. The IC_{50} values were further converted to the inhibition constant K_i values by using the Cheng–Prusoff equation (Equation (2)).[68]

$$K_i = \frac{IC_{50}}{1 + \left(\frac{[S]}{K_m}\right)} \quad (2)$$

As shown in Equation (2), $[S]$ is the substrate concentration and K_m ((0.28 ± 0.04) μM) is the Michaelis constant of the substrate for the enzyme obtained from a Micahelis–Menten plot (see Figure S1 in the Supporting Information).

The Lineweaver–Burk analysis was carried out by using different substrate and inhibitor concentrations with a range of 0.1–1 μM and 0.1–5.0 μM, respectively. In all the cases, the GGPP concentration was fixed to 5 μM for the saturated condition. The Lineweaver–Burk plot of $1/v$ versus $1/[S]$ was analyzed by competitive, noncompetitive, and uncompetitive models with SigmaPlot and the best fit was obtained by a competitive model in which the initial velocity v is given by Equation (3).

$$v = \frac{V_{max}}{1 + \left(\frac{K_m}{[S]}\right)\left(1 + \frac{[I]}{K_i}\right)} \quad (3)$$

In Equation (3), v is arbitrary fluorescence units per second, V_{max} is the maximum velocity of the reaction, and $[I]$ is the inhibitor concentration.

In vitro GGTase I and FTase activity assays with [^{3}H]-labeled substrates: In vitro inhibition assays of mammalian FTase and GGTase I were performed by measuring the incorporation of [^{3}H] FPP (GE Healthcare, Piscataway, NJ) and [^{3}H] GGPP (Perkin-Elmer Life Sciences, Boston, MA) into wild-type H-Ras (FTase) and H-Ras-CVLL (GGTase I), respectively, as previously described.[71] Briefly, approximately 20μg of 60000×g postmicrosomal supernatant from SF-9 cells expressing human GGTase I or FTase was incubated in the presence of an increasing concentration of compound, 10 μg H-Ras or H-Ras-CVLL substrate, and 0.5 μCi/sample of either [^{3}H] FPP or [^{3}H] GGPP. Samples were precipitated by using trichloroacetic acid (TCA) and then filtered onto glass-fiber filters; unbound [^{3}H] FPP or [^{3}H] GGPP was washed through the filters. Samples were counted in a scintillation counter and the activity was compared with vehicle controls to obtain IC_{50} values.

Acknowledgements

Financial support from Hayashi Memorial Foundation and a Grant-in-Aid from the Ministry of Education, Culture, Sports, Science and Technology is acknowledged. We are grateful to Professor Patrick Casey for providing us the plasmids. J.O. sincerely thanks Professors Andrew Hamilton and Indraneel Ghosh for helpful discussions.

[1] P. Bork, L. J. Jensen, C. V. Merg, A. K. Ramani, I. Lee, E. M. Marcotte, *Curr. Opin. Struct. Biol.* **2004**, *14*, 292–299.
[2] B. P. Orner, J. T. Ernst, A. D. Hamilton, *J. Am. Chem. Soc.* **2001**, *123*, 5382–5383.
[3] S. Fletcher, A. D. Hamilton, *Curr. Opin. Chem. Biol.* **2005**, *9*, 632–638.
[4] H. Yin, A. D. Hamilton, *Angew. Chem.* **2005**, *117*, 4200–4235; *Angew. Chem. Int. Ed.* **2005**, *44*, 4130–4163.
[5] L. Pagliaro, J. Felding, K. Audouze, S. J. Nielsen, R. B. Terry, C. Krog-Jensen, S. Bucher, *Curr. Opin. Chem. Biol.* **2004**, *8*, 442–449.
[6] M. R. Arkin, J. A. Wells, *Nat. Rev. Drug Discovery* **2004**, *3*, 301–317.
[7] J. A. Kritzer, R. Zutshi, M. Cheah, F. A. Ran, R. Webman, T. M. Wongjirad, A. Schepartz, *ChemBioChem* **2006**, *7*, 29–31.
[8] S. E. Rutledge, H. M. Volkman, A. Schepartz, *J. Am. Chem. Soc.* **2003**, *125*, 14336–14347.
[9] S. Rajagopal, S. C. Meyer, A. Goldman, M. Zhou, I. Ghosh, *J. Am. Chem. Soc.* **2006**, *128*, 14356–14363.
[10] T. J. Smith, C. I. Stains, S. C. Meyer, I. Ghosh, *J. Am. Chem. Soc.* **2006**, *128*, 14456–14457.
[11] R. L. A. Dias, R. Fasan, K. Moehle, A. Renard, D. Obrecht, J. A. Robinson, *J. Am. Chem. Soc.* **2006**, *128*, 2726–2732.
[12] Y. Hamuro, M. Calama, H. Park, A. D. Hamilton, *Angew. Chem.* **1997**, *109*, 2797–2800; *Angew. Chem. Int. Ed.* **1997**, *36*, 2680–2683.
[13] H. S. Park, Q. Lin, A. D. Hamilton, *Proc. Natl. Acad. Sci. USA* **2002**, *99*, 5105–5109.
[14] H. C. Zhou, L. Baldini, J. Hong, A. J. Wilson, A. D. Hamilton, *J. Am. Chem. Soc.* **2006**, *128*, 2421–2425.
[15] K. Groves, A. J. Wilson, A. D. Hamilton, *J. Am. Chem. Soc.* **2004**, *126*, 12833–12842.
[16] R. K. Jain, A. D. Hamilton, *Org. Lett.* **2000**, *2*, 1721–1723.
[17] J. E. Gestwicki, G. R. Crabtree, I. A. Graef, *Science* **2004**, *306*, 865–869.
[18] S. L. Hussey, S. S. Muddana, B. R. Peterson, *J. Am. Chem. Soc.* **2003**, *125*, 3692–3693.
[19] D. A. Erlanson, J. W. Lam, C. Wiesmann, T. N. Luong, R. L. Simmons, W. L. Delano, I. C. Choong, M. T. Burdett, W. M. Flanagan, D. Lee, E. M. Gordon, T. O'Brien, *Nat. Biotechnol.* **2003**, *21*, 308–314.
[20] Y. Takaoka, H. Tsutsumi, N. Kasagi, E. Nakata, I. Hamachi, *J. Am. Chem. Soc.* **2006**, *128*, 3273–3280.
[21] J. Dimaio, B. Gibbs, D. Munn, J. Lefebvre, F. Ni, Y. Konishi, *J. Biol. Chem.* **1990**, *265*, 21698–21703.
[22] T. Steinmetzer, B. Y. Zhu, Y. Konishi, *J. Med. Chem.* **1999**, *42*, 3109–3115.
[23] K. M. Jude, A. L. Banerjee, M. K. Haldar, S. Manokaran, B. Roy, S. Mallik, D. K. Srivastava, D. W. Christianson, *J. Am. Chem. Soc.* **2006**, *128*, 3011–3018.
[24] A. L. Banerjee, M. Swanson, B. C. Roy, X. Jia, M. K. Haldar, S. Mallik, D. K. Srivastava, *J. Am. Chem. Soc.* **2004**, *126*, 10875–10883.

[25] K. Enander, G. T. Dolphin, L. Baltzer, *J. Am. Chem. Soc.* **2004**, *126*, 4464–4465.
[26] B. A. Grzybowski, A. V. Ishchenko, C. Y. Kim, G. Topalov, R. Chapman, D. W. Christanson, G. M. Whitesides, E. I. Shakhnovich, *Proc. Natl. Acad. Sci. USA* **2002**, *99*, 1270–1273.
[27] P. A. Boriack, D. W. Christianson, J. Kingery-Wood, G. M. Whitesides, *J. Med. Chem.* **1995**, *38*, 2286–2291.
[28] N. Schaschke, D. Gabrijelcic-Geiger, A. Dominik, C. P. Sommerhoff, *ChemBioChem* **2005**, *6*, 95–103.
[29] K. Shen, P. A. Cole, *J. Am. Chem. Soc.* **2003**, *125*, 16172–16173.
[30] A. Profit, A. T. R. Lee, D. S. Lawrence, *J. Am. Chem. Soc.* **1999**, *121*, 280–283.
[31] B. C. Roy, A. L. Banerjee, M. Swanson, X. G. Jia, M. K. Haldar, S. Mallik, D. K. Srivastava, *J. Am. Chem. Soc.* **2004**, *126*, 13206–13207.
[32] M. C. Seabra, Y. Reiss, P. J. Casey, M. S. Brown, *Cell* **1991**, *65*, 429–434.
[33] W. W. Epstein, D. Lever, L. M. Leining, E. Bruenger, H. C. Rilling, *Proc. Natl. Acad. Sci. USA* **1991**, *88*, 9668–9670.
[34] P. J. Casey, *J. Lipid Res.* **1992**, *33*, 1731–1740.
[35] K. Zhu, A. D. Hamilton, S. M. Sebti, *Curr. Opin. Invest. Drugs* **2003**, *4*, 1428–1435.
[36] F. G. Njoroge, A. G. Taveras, J. Kelly, S. Remiszewski, A. K. Mallams, R. Wolin, A. Afonso, A. B. Cooper, D. F. Rane, Y. T. Liu, J. Wong, B. Vibulbhan, P. Pinto, J. Deskus, C. S. Alvarez, J. D. Rosario, M. Connolly, J. Wang, J. Desai, R. R. Rossman, W. R. Bishop, R. Patton, L. Wang, P. Kirschmeier, M. S. Bryant, A. A. Nomeir, C. C. Lin, M. Liu A. T. McPhail, R. J. Doll, V. M. Girijavallabhan, A. K. Ganguly, *J. Med. Chem.* **1998**, *41*, 4890–4902.
[37] L. Wang, G. T. Wang, X. Wang, Y. Tong, G. Sullivan, D. Park, N. M. Leonard, Q. Li, J. Cohen, W. Gu, H. Zhang, J. L. Bauch, C. G. Jakob, C. W. Hutchins, V. S. Stoll, K. Marsh, S. H. Rosenberg, H. L. Sham, N. Lin, *J. Med. Chem.* **2004**, *47*, 612–626.
[38] A. D. Basso, P. Kirschmeier, W. R. Bishop, *J. Lipid Res.* **2006**, *47*, 15–31.
[39] M. H. Gelb, L. Brunsveld, C. A. Hrycyna, S. Michaelis, F. Tamanoi, W. C. V. Boorhis, H. Waldmann, *Nat. Chem. Biol.* **2006**, *2*, 518–528.
[40] M. R. Philips, A. D. Cox, *J. Clin. Invest.* **2007**, *117*, 1223–1225.
[41] J. Sun, J. Ohkanda, D. Coppola, H. Yin, M. Kothare, B. Busciglio, A. D. Hamilton, S. M. Sebti, *Cancer Res.* **2003**, *63*, 8922–8929.
[42] Y. K. Peterson, P. Kelly, C. A. Weinbaum, P. J. Casey, *J. Biol. Chem.* **2006**, *281*, 12445–12450.
[43] H. Peng, D. Carrico, V. Thai, M. A. Blaskovich, C. Bucher, E. E. Pusateri, S. M. Sebti, A. D. Hamilton, *Org. Biomol. Chem.* **2006**, *4*, 1768–1784.
[44] A. M. Sjogren, K. M. Andersson, M. Liu, B. A. Cutts, C. Karlsson, A. M. Wahlstrom, M. Dalin, C. Weinbaum, P. J. Casey, A. Tarkowski, B. Swolin, S. G. Young, M. O. Bergo, *J. Clin. Invest.* **2007**, *117*, 1294–1304.
[45] S. Castellano, H. D. G. Fiji, S. S. Kinderman, M. Watanabe, P. D. Leon, F. Tamanoi, O. Kwon, *J. Am. Chem. Soc.* **2007**, *129*, 5843–5845.
[46] B. S. Zuckerbraun, J. E. Barbato, A. Hamilton, S. Sebti, E. Tzeng, *J. Surg. Res.* **2005**, *124*, 256–263.
[47] J. Ye, C. Wang, J. Rhea Sumpter, M. S. Brown, J. L. Goldstein, J. Michael Gale, *Proc. Natl. Acad. Sci. USA* **2003**, *100*, 15865–15870.
[48] R. Khosravi-Far, P. A. Solski, G. J. Clark, M. S. Kinch, C. J. Der, *Mol. Cell. Biol.* **1995**, *15*, 6443–6453.
[49] E. A. Clark, T. R. Golub, E. S. Lander, R. O. Hynes, *Nature* **2000**, *406*, 532–535.
[50] P. L. Joyce, A. D. Cox, *Cancer Res.* **2003**, *63*, 7959–7967.
[51] R. G. Qiu, A. Abo, F. McCormick, M. Symons, *Mol. Cell. Biol.* **1997**, *17*, 3449–3458.
[52] K. Lim, A. T. Baines, J. J. Fiordalisi, M. Shipitsin, L. A. Feig, A. D. Cox, C. J. Der, C. M. Counter, *Cancer Cell* **2005**, *7*, 533–545.
[53] E. C. Lerner, Y. M. Qian, A. D. Hamilton, S. M. Sebti, *J. Biol. Chem.* **1995**, *270*, 26770–26773.
[54] D. B. Whyte, P. Kirschmeier, T. N. Hockenberry, I. Nunez-Oliva, L. James, J. J. Catino, W. R. Bishop, J. Pai, *J. Biol. Chem.* **1997**, *272*, 14459–14464.
[55] C. A. Rowell, J. J. Kowalczyk, M. D. Lewis, A. M. Garcia, *J. Biol. Chem.* **1997**, *272*, 14093–14097.
[56] K. L. Terry, P. J. Casey, L. S. Beese, *Biochemistry* **2006**, *45*, 9746–9755.
[57] T. S. Reid, S. B. Long, L. S. Beese, *Biochemistry* **2004**, *43*, 9000–9008.
[58] J. S. Taylor, T. S. Reid, K. L. Terry, P. J. Casey, L. S. Beese, *EMBO J.* **2003**, *22*, 5963–5974.
[59] G. L. James, J. L. Goldstein, M. S. Brown, *J. Biol. Chem.* **1995**, *270*, 6221–6226.
[60] F. L. Zhang, P. Kirschmeier, D. Carr, L. James, R. W. Bond, L. Wang, R. Patton, W. Windsor, R. Syto, R. Zhang, W. R. Bishp, *J. Biol. Chem.* **1997**, *272*, 10232–10239.
[61] S. B. Long, P. J. Casey, L. S. Beese, *Structure* **2000**, *8*, 209–222.
[62] I. Smalera, J. M. Williamson, W. Baginsky, B. Leiting, P. Mazur, *Biochim. Biophys. Acta* **2000**, *1480*, 132–144.
[63] K. T. Lane, L. S. Beese, *J. Lipid Res.* **2006**, *47*, 681–699.
[64] T. S. Reid, K. L. Terry, P. J. Casey, L. S. Beese, *J. Mol. Biol.* **2004**, *343*, 417–433.
[65] S. L. Moores, M. D. Schaber, S. D. Mosser, E. Rands, M. B. O'Hara, V. M. Garsky, M. S. Marshall, D. L. Pompliano, J. B. Gibbs, *J. Biol. Chem.* **1991**, *266*, 14603–14610.
[66] W. G. Stirtan, C. D. Poulter, *Biochemistry* **1997**, *36*, 4552–4557.
[67] H. Fu, J. F. Moomaw, C. R. Moomaw, P. J. Casey, *J. Biol. Chem.* **1996**, *271*, 28541–28548.
[68] Y. Cheng, W. H. Prusoff, *Biochem. Pharmacol.* **1973**, *22*, 3099–3108.
[69] D. K. Srivastava, K. M. Jude, A. L. Banerjee, M. Haldar, S. Manokaran, J. Kooren, S. Mallik, D. W. Christianson, *J. Am. Chem. Soc.* **2007**, *129*, 5528–5537.
[70] P. Broto, G. Moreau, C. Vandycke, *Eur. J. Med. Chem.* **1984**, *19*, 71–78.
[71] A. Vogt, Y. Qian, T. F. McGuire, A. D. Hamilton, S. M. Sebti, *Oncogene* **1996**, *13*, 1991–1999.
[72] S. B. Long, P. J. Hancock, A. M. Kral, H. W. Hellinga, L. S. Beese, *Proc. Natl. Acad. Sci. USA* **2001**, *98*, 12948–12953.

Received: October 15, 2007
Revised: November 28, 2007
Published online: January 17, 2008

Journal of Peptide Science
J. Pept. Sci. (2008)
Published online in Wiley InterScience (www.interscience.wiley.com). DOI: 10.1002/psc.1021

JOURNAL OF PEPTIDE SCIENCE

Short Communication

Facile detection of specific RNA-polypeptide interactions by MALDI-TOF mass spectrometry

MAKI SUGAYA,[a] RYOTA SAITO,[a] YURIKO MATSUMURA,[a] KAZUO HARADA[b] and AKIRA KATOH[a]*

[a] Department of Materials and Life Science, Faculty of Science and Technology, Seikei University, Musashino, Tokyo 180-8633, Japan
[b] Department of Life Science, Tokyo Gakugei university, Tokyo 184-8501, Japan

Received 19 September 2007; Revised 20 December 2007; Accepted 21 December 2007

Abstract: A simple method for the detection of specific RNA-polypeptide interactions using MALDI-TOF mass spectroscopy is described. Instead of direct observation of the RNA-polypeptide complex, we attempted the indirect observation of the binding event by focusing on the disappearance of the free polypeptide signal upon interaction with RNA. As a result, specific binding of the Rev-response element (RRE) RNA of the HIV with two RRE-binding peptide aptamers, DLA and RLA peptides, as well as the bacteriophage λ boxB RNA with the λ N peptide was observed. We also show that specific RNA-binding peptides can be identified from a mixture of peptides with varying RNA-binding affinity, showing that the method could be applied to high-throughput screening from simple peptide libraries. The method described in this study provides a quick and simple method for detecting specific RNA–polypeptide interactions that avoids difficulties associated with direct observation of RNA and RNA–polypeptide complexes, which may find various applications in the analysis of RNA–polypeptide interactions and in the identification of novel RNA-binding polypeptides. Copyright © 2008 European Peptide Society and John Wiley & Sons, Ltd.

Supplementary electronic material for this paper is available in Wiley InterScience at http://www.interscience.wiley.com/jpages/1075-2617/suppmat/

Keywords: RNA–polypeptide interactions; MALDI-TOF mass spectrometry; arginine-rich peptide; HIV RRE; lambda boxB; peptide library

INTRODUCTION

RNA–polypeptide interactions are intimately involved in various steps of gene regulation, and various methods for the detection and analysis of RNA–polypeptide interactions have been developed. However, *in vitro* methods such as calorimetry, gel mobility shift assays, surface plasmon resonance (SPR) require large quantities of substrate or radioactive/fluorescent labeling of either the RNA or polypeptide. Genetic methods for detecting RNA–polypeptide interactions such as the three-hybrid system [1] and the antitermination system [2] require cloning of sequences encoding the RNA and polypeptide of interest into plasmid vectors and yeast/bacterial culture. The development of simple methods for the detection of RNA–polypeptide complexes would be expected to facilitate the analysis of RNA–polypeptide interactions, and the identification of novel RNA-binding polypeptides.

The development of soft ionizing methods in mass spectrometry has made possible the simple and rapid detection of biological samples including RNA. MALDI-TOF mass spectrometry is the easiest and the most widely available method for the analysis of RNA [3]. However, in addition to the generally inefficient desorption of RNA, a number of difficulties that are common for oligonucleotides exist for the analysis of RNA. First, sample preparation is a key step in RNA analysis, as impurities can result in reduced sensitivity [4]. The choice of the proper combination of matrix material has been shown to be crucial for successful analysis, and 3-hydroxypicolinic acid (3-HPA) [5] and 2,4,6-trihydroxyacetophenone (2,4,6-THAP) [6] in combination with organic ammonium salts were found to be useful matrices. Organic ammonium salts such as ammonium citrate and ammonium tartrate were shown to suppress addition of alkali metals, which lead to the division of the molecular ion into multiple peaks ([M + Na] and [M + K]) and a reduction in resolution [6,7]. Ammonium salts have also been shown to suppress fragmentation of the oligonucleotides [7]. The 5′- and 3′-heterogeneity of T7 RNA transcripts has also been to implicated as a source of peak widening and low resolution [8]. Despite these advances, however, the sensitivity of RNA detection is much reduced compared to analysis of polypeptides of

*Correspondence to: Akira Katoh, Department of Materials and Life Science, Faculty of Science and Technology, Seikei University, Kitamachi 3-3-1, Kichijoji, Musashino-shi, Tokyo 180-8633, Japan;
e-mail: katoh@st.seikei.ac.jp

comparable size. While there has been a report that an enzymatically synthesized RNA of 461 nucleotides could be detected [8], there are few examples of the analysis of oligomers longer than 20 nucleotides.

In this study, the development of a novel method for the facile detection of specific RNA-polypeptide interactions by MALDI-TOF MS was attempted. While the detection of non-covalently linked complexes of short RNAs (9 to 19 nucleotides) and peptides (10 to 18 amino acids) has already been reported [9], simple and convenient analysis of such complexes was expected to be hampered by the difficulties associated with RNA as described above. We therefore focused on the disappearance of the signal for the more readily detectable polypeptide upon specific binding to RNA. In other words, it was expected that the signal for the RNA-binding peptide would not be detected when bound specifically to the RNA, while those peptides that do not bind specifically to the RNA would be observed, resulting in the indirect observation of specific RNA-polypeptide complex formation.

A 34-nucleotide RNA stem-loop from the Rev-response element (RRE) of HIV and RRE-binding peptides (DLA and RLA peptides) with differing affinities for the RRE [10], as well as the 19-mer boxB RNA from phage λ and the λ N peptide [11] were used as model RNA–polypeptide complexes (Figure 1). Using MALDI-TOF MS, it was shown, as expected, that specific RNA-binding by RRE-binding peptides and the λ N peptide could be observed by the disappearance of the peptide signal upon mixing with RNA. It was also shown that the identification of RNA-binding peptides from mixtures of peptides with differing RNA-binding affinity is possible.

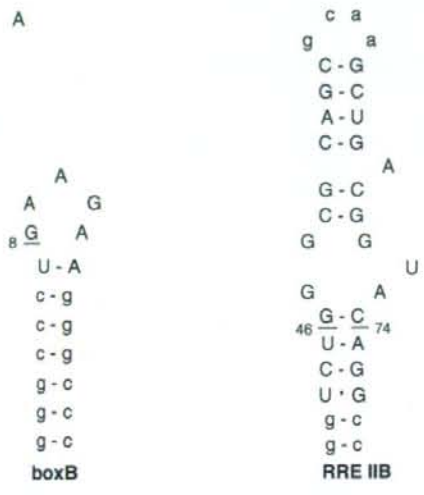

Figure 1 RNAs and RNA-binding peptide. (A) Secondary structures of the boxB RNA and the RRE IIB RNA. The underlined nucleotides are substituted in mutant RNAs. (B) RNA-binding peptides. The DLA and RLA peptides bind to RRE, the N peptide binds to boxB RNA. The underlined amino acids were not included in the synthetic peptide.

RESULTS AND DISCUSSION

Confirmation of RNA-peptide Interactions Using a Bacterial Reporter System

The interactions of the RNAs and peptides used in the present study were confirmed using a bacterial reporter system that utilizes the bacteriophage λ N protein mediated antitermination to monitor RNA–polypeptide interaction (Table 1) [2]. The pBR plasmids encoding the DLA, RLA or λ N peptides were transformed into pAC LacZ reporter cells encoding either the RRE or boxB RNA (Figure 1), and antitermination activity was assayed on tryptone plates containing X-gal. The intensity of colony color represented as plusses has been shown to correlate with binding affinity, where the interaction between the RRE RNA and the DLA peptide (Kd = 0.5 nM) reports an antitermination activity of 6+ [10], while that of the RRE and the RLA peptide (Kd = 30 nM) was 3.5+ [10], and that of the λ boxB RNA and the λ N peptide (Kd = 20 nM) was 8+ [11]. On

Table 1 The *in vivo* activities (X-gal assay) and Kd values (nM) of the DLA, RLA, λ N peptides with the boxB and RRE IIB

	X-gal (Kd, nM)[a]					
	DLA		RLA		λ N	
RRE	++++++	(0.5)	+++(+)	(30)	—	
RRE C46G74						
boxB	—		—		++++++++	(20)
boxB G8A						(>2560)

[a] The number of plusses indicates blue color scored by the colony color (X-gal) assay.

the other hand, the interaction between the RRE and the λ N peptide, as well as the interaction between the boxB with both the DLA and RLA peptides did not show antiterrmination activity, and could not be detected.

Optimization of the Matrix Material for RNA and Polypeptide Detection

A number of different matrices, α-cyano-4-hydroxycinnamic acid (CHCA), 2,5-dihydroxybenzoic acid (DHB), 3-HPA, 2,3,4-THAP and 2,4,6-THAP, were tested for the analysis of the above mentioned RNAs, peptides and RNA–peptide complexes in both the negative and positive-ion mode. CHCA is widely used for the analysis of various materials [12], and DHB is used for DNA and sugar analysis [13].

All measurements were repeated three times and contained a synthetic peptide, P14R peptide (MW 1534) or angiotensin II (MW 1046), as an internal standard. Ammonium citrate was included to suppress addition of alkali metals. Only peaks of the peptides were observed clearly with CHCA, DHB and 2,4,6-THAP, and were similar in both ion modes. The signals of the RNAs were weak with all matrices, and the RNA–peptide complex, RRE–DLA complex, could only be detected with 2,4,6-THAP in positive-ion mode. Therefore, all of the following mass analyses were performed with 2,4,6-THAP in the positive-ion mode.

The Detection of RNA-polypeptide Complex Formation by the Disappearance of the Free-Peptide Signal

We tried to detect RNA–peptide complex formation by monitoring the decrease of the signal corresponding to the peptide, using the P14R peptide as an internal standard. When ammonium citrate and 2,4,6-THAP were added immediately after mixing the RRE RNA and the DLA peptide to form a solid solution, the peak of the free peptide was observed (Figure 2(A)). When ammonium citrate and 2,4,6-THAP were added after a 10-min incubation of the RNA and peptide at room temperature or on ice, followed by solid solution formation, the peak of the RNA-binding peptide was not detected (Figure 2(B)). In addition, the intensity of the peak corresponding to the DLA peptide decreased as the molar ratio of RRE RNA added was gradually increased in 0.25 molar equivalent increments (Figure S1, supporting data). This suggested that, as expected, upon binding of the DLA peptide with the RRE RNA, the DLA peptide was no longer released upon laser desorption, thereby providing a means to indirectly detect the RNA–peptide binding event. Therefore, all of the following mass analyses were performed after a ten-minute incubation of the mixture of RNA and peptide at room temperature.

The Detection of Specific RNA-peptide Interactions

First, the interaction of HIV RRE RNA and RRE-binding peptides was examined. When a mixture of the DLA peptide, which binds to RRE with high affinity and high specificity (Kd = 0.5 nM, Table 1), was analyzed, the DLA peptide showed a mass peak with an intensity comparable to that of P14R, the internal standard (Figure 3(A)). In comparison, upon addition of the RRE RNA to this mixture, a complete disappearance of the signal corresponding to the DLA peptide was observed, while the peak of the P14R peptide remained unchanged (Figure 3(B)), as also observed in Figure 2(B). On the other hand, when an RRE mutant (C46G74) that does not bind to the DLA peptide was added, no effect on the DLA signal was observed (Figure 3(C)). This suggested that the disappearance of the DLA peak upon addition of the wild-type RRE represented a specific binding event, and was not due to non-specific binding. Next, when a mixture of the RRE RNA and the RLA peptide, which binds to the RRE with a Kd of 30 nM (Table 1), was analyzed, the peak corresponding to the RLA peptide disappeared (Figure 3(D), (E)). Furthermore, as in the case of the DLA peptide described above, the signal corresponding

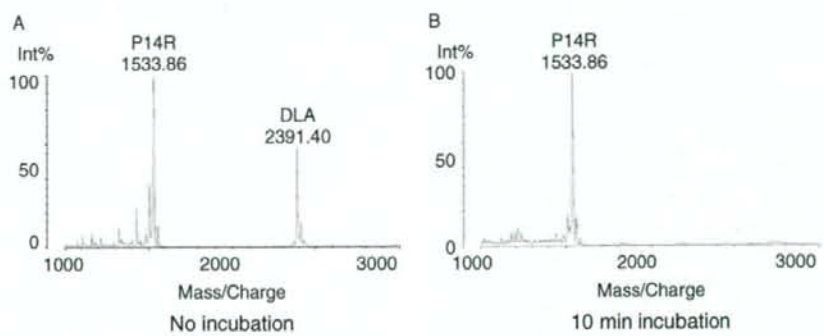

Figure 2 MALDI-TOF mass spectra of DLA peptide-RRE RNA. (A) No incubation (B) 10-min incubation. This figure is available in colour online at www.interscience.wiley.com/journal/jpepsci.

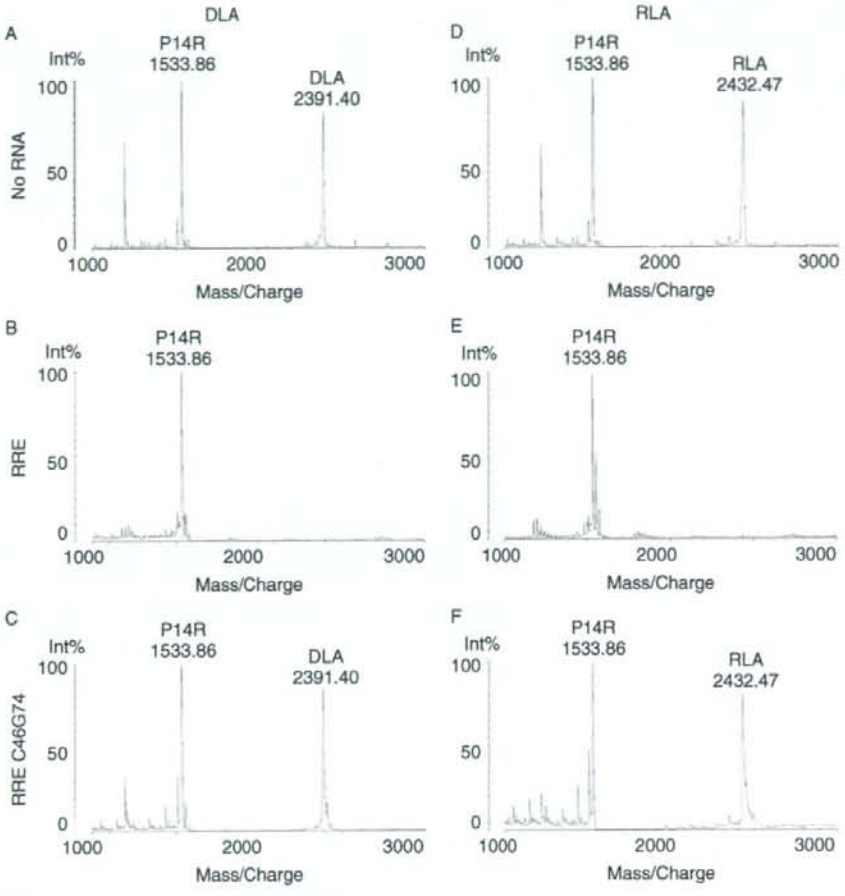

Figure 3 MALDI-TOF mass spectra of the free peptides and mixtures of the peptides and RRE RNA or RRE C46G74 RNA. (A) DLA peptide (B) DLA peptide-RRE RNA (C) DLA peptide-RRE C46G74 RNA (D) RLA peptide (E) RLA peptide-RRE RNA (F) RLA peptide-RRE C46G74 RNA. This figure is available in colour online at www.interscience.wiley.com/journal/jpepsci.

to the RLA peptide did not disappear upon addition of the RRE mutant (Figure 3(F)), showing that specific RNA–polypeptide interactions with a Kd of at least more than 30 nM could be analyzed by this method. As expected, addition of the wild-type and mutant RRE to the λ N peptide, which does not bind specifically to the RRE, resulted in no change in the peptide signal (Figure S2, supporting data).

In order to confirm that specific binding of the λ N peptide with the boxB RNA could also be observed by this method, the interaction of the DLA, and RLA, and λ N peptides with the wild-type boxB and a mutant boxB was analyzed (Figures 4 and S3, supporting data). Addition of the wild-type and mutant boxB RNAs to the DLA and RLA peptides resulted in the retention of the signals corresponding to the peptides (Figure S3(A)–(F), supporting data). On the other hand, addition of the wild-type box B to the λ N peptide resulted in an almost complete disappearance of the signal corresponding to the peptide, while the addition of the mutant boxB (G8A) did not affect the peptide signal (Figure 4). This further confirmed that specific RNA-polypeptide binding could be simply detected by whether or not the free-peptide signal in the MALDI-TOF MS vanishes upon RNA addition.

Identification of Specific RNA-binding Peptides from a Simple Peptide Library

In order to elucidate the utility of the present technique to identify RNA-binding peptides from mixtures of peptides with varying RNA-binding affinities, mixtures of peptides were treated with either the RRE or the RRE mutant (Figure 5). As a result, for example, when the DLA, RLA and λ N peptides were mixed with the RRE, only the signals corresponding to the DLA and RLA peptide disappeared (Figure 5(B)), while both the signals were present when the RRE mutant was used (Figure 5(C)).

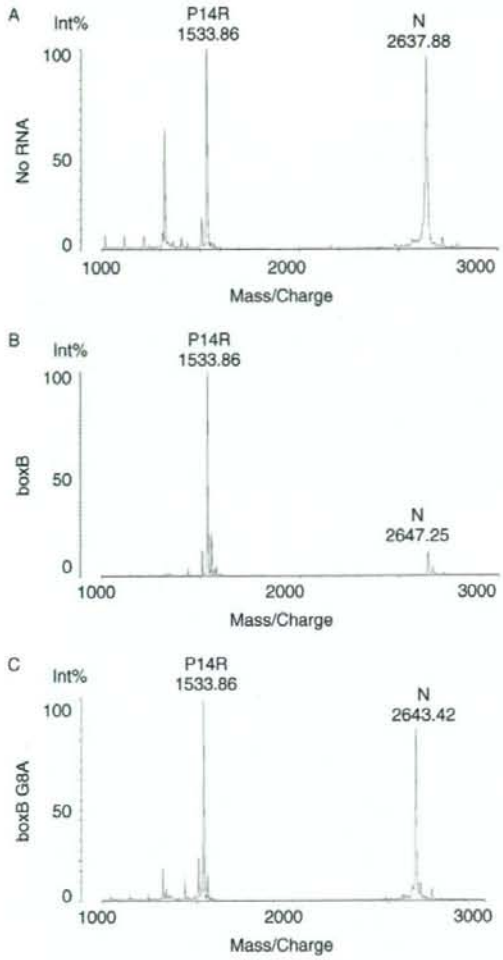

Figure 4 MALDI-TOF mass spectra of the free peptide and mixtures of the peptide and boxB RNA or boxB G8A RNA. (A) λ N peptide (B) λ N peptide-boxB RNA (C) λ N peptide-boxB G8A RNA. This figure is available in colour online at www.interscience.wiley.com/journal/jpepsci.

CONCLUSIONS

A simple method for detecting specific RNA–polypeptide interactions by MALDI-TOF MS that avoids difficulties associated with the direct analysis of the RNA-polypeptide complex, and is expected to be useful in the qualitative analysis of RNA-polypeptide interactions is described. The ability to identify strongly binding peptides from a mixture of similar peptides with varying RNA affinity, combined with the ease with which analysis can be carried out, suggests that MALDI-TOF MS may be applicable for the high-throughput screening of specific RNA-binder from simple peptide libraries.

MATERIALS AND METHODS

The Preparation of RNAs and Peptides

The RNAs were prepared by *in vitro* transcription using T7 RNA polymerase of synthetic oligonucleotide templates for RRE (5′-GGCCTGTACCGTCAGCTTGCGCTGCGCCCAGACCTATAG-TGAGTCGTATTAC-3′), RRE C46G74 (5′-GGCCTCTACCGTCA-GCTTGCGCTGCGCCCAGACCTATAGTGAGTCGTATTAC-3′), boxB (5′-GGGCCCTTCTTCAGGGCCCTATAGTGAGTCGTAT-TAC-3′), and boxB G8A (5′-GGGCCCTTCTTTAGGGCCCTATA-GTGAGTCGTATTAC-3′) that were annealed to the T7 primer (5′-GTAATACGACTCACTATA-3′). The RNA oligonucleotides were purified in denaturing PAGE, and desalted on a NAP 5 columns (Amersham Biosiences). The RNA was dissolved in H_2O to 100 pmol/μl, and were annealed by heating at 95°C for 5 min and quick-cooling to 0°C. The arginine-rich peptides were constructed on XX resin using automatic peptide synthesizer (Applied Biosystems, Model 433A) starting from Fmoc-Arg(pmc)-resin (0.25 mmol/g) with standard Fmoc-chemistry. The peptides were deprotected and cleaved from the resin by the treatment with TFA for 4 h at room temperature. The peptides were isolated and purified by HPLC with linear gradient conditions of acetonitrile/H2O/0.1% TFA as eluent. The peptides were lyophylized as fluffy white powder of the acetates and analyzed by MALDI-TOF MS using Voyger Linear II. The [M + H] cations were detected for all synthetic peptides. The λ N peptide used in this study was shorter by four amino acid residues at *C*-terminal than that used for gel shift (Figure 1). These amino acid residues are not important for binding to boxB RNA [14].

Mass Spectrometric Analysis

The matrices CHCA, DHB, 3-HPA were obtained from SIGMA-ALDRICH, and 2,4,6-THAP was obtained from Fluka. Ammonium citrate was obtained from SIGMA-ALDRICH.

One microliter of the RNA and 1 μl of the peptide (100 pmol/μl in H_2O), in the case of the mixtures of RRE or RRE C46G74 RNAs and all peptides, 3 μl of the RNA (100 pmol/μl) and 0.1 μl of the peptide (1 nmol/μl in H_2O) were incubated together in a 1.5-ml tube for 10 min at room temperature (20°C) or on ice. Following the addition of 0.5 μl of 0.2 N ammonium citrate and 0.5 μl of ProteoMass P14R MALDI-MS Standard (SIGMA-ALDRICH), each sample was dropped on a sample plate. Then, the matrix solution 1.2 μl of 20 mg/ml 2,4,6-THAP in methanol, 1 μl of 15 mg/ml DHB in 0.1% TFA/acetonitrile (2 : 1) or 1.2 μl of 60 mg/ml 3-HPA in H_2O, was dropped on the sample very carefully, and dried. After drying the spots on the plate completely, the mass analysis performed with Axima CFRplus MALDI-TOF MS spectrometer (Shimadzu, Japan). Each spectrum was averaged for 100 laser shots in linear mode at 120 mV.

RNA-peptides Binding Assay *in Vivo*

pBR plasmid DNAs activities were monitored using the LacZ colony color assay [2] with N567/reporter cells containing pAC-RRE or pAC-λ nut plasmids. N567/pAC cells (50 μl) were transformed using 1 μl of the pBR plasmid DNA (10 ng) by heat shock, and incubated in the tryptone medium (0.5 ml) at 37°C for 1 h. A portion of the culture was spread onto

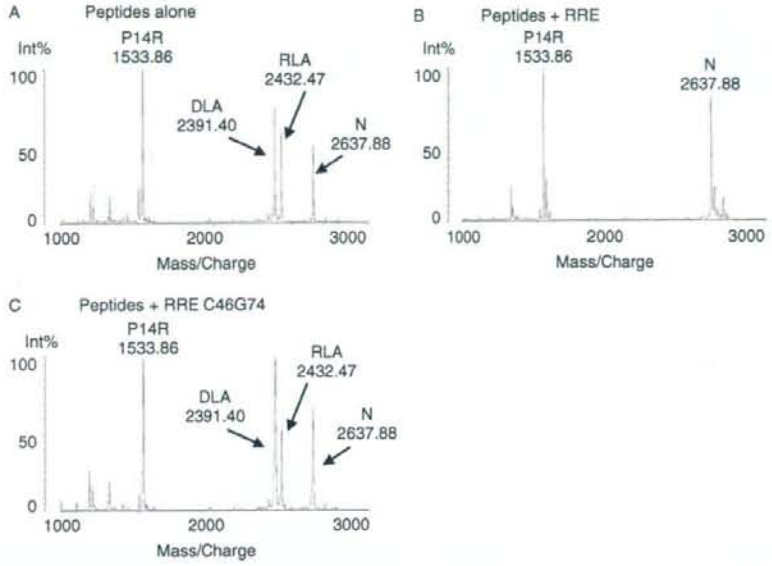

Figure 5 MALDI-TOF mass spectra of mixed peptides and RRE RNA or RRE C46G74 RNA. (A) DLA, RLA, and λ N peptides (B) DLA, RLA, and λ N peptides-RRE RNA (C) DLA, RLA, and λ N peptides-RRE C46G74 RNA. This figure is available in colour online at www.interscience.wiley.com/journal/jpepsci.

tryptone plates (60 mm diameter) containing 100 μg/ml ampicillin, 20 μg/ml chloramphenicol, 0.05 mM IPTG, 80 μg/ml 5-bromo-4-chloro-3-indolyl-β-D- galactopyranoside (X-gal), incubated at 37 °C for 24 h, and the proportion of blue colonies was scored [2].

Supplementary Material

Supplementary electronic material for this paper is available in Wiley InterScience at: http://www.interscience.wiley.com/jpages/1075-2617/suppmat/

Acknowledgements

This work was supported in part by a Grant-in-Aid Research in Priority Areas from the Ministry of Education, Culture, Sports, Science and Technology (MEXT) of Japan, and by 'High-Tech Research Center' Project for private universities: matching fund subsidy from MEXT (2004-2008).

REFERENCES

1. SenGupta DJ, Zhang B, Kraemer B, Pochart P, Fields S, Wickens M. A three-hybrid system to detect RNA-protein interactions in vivo. *Proc. Natl. Acad. Sci. U.S.A.* 1996; **93**: 8496–8501.
2. Harada K, Martin SS, Frankel AD. Selection of RNA-binding peptides *in vivo*. *Nature* 1996; **380**: 175–179.
3. Thomas B, Akoulitchev AV. Mass spectrometry of RNA. *Trends Biochem. Sci.* 2006; **31**: 173–181.
4. Shaler TA, Wickham JN, Sannes KA, Wu KJ, Becker CH. Effect of impurities on the matrix-assisted laser desorption mass spectra of single-stranded oligodeoxynucleotides. *Anal. Chem.* 1996; **68**: 576–579.
5. Wu KJ, Steding A, Becker CH. Matrix-assisted laser desorption time-of-flight mass spectrometry of oligonucleotides using 3-hydroxypicolinic acid as an ultraviolet-sensitive matrix. *Rapid Commun. Mass Spectrom.* 1993; **7**: 142–146.
6. Pieles U, Zürcher W, Schär M, Moser HE. Matrix-assisted laser desorption ionization time-of-flight mass spectrometry: a powerful tool for the mass and sequence analysis of natural and modified oligonucleotides. *Nucleic Acids Res.* 1993; **21**: 3191–3196.
7. Zhu YF, Chung CN, Taranenco NI, Allman SL, Martin SA, Haff L, Chen CH. The study of 2,3,4-trihydroxyacetophenone and 2,4,6-trihydroxyacetophenone as matrices for DNA detection in matrix-assisted laser desorption/ionization time-of-flight mass spectrometry. *Rapid Commun. Mass Spectrom.* 1996; **10**: 383–388.
8. Kirpekar F, Nordhoff E, Kristiansen K, Roepstorff P, Lezius A, Hahner S, Karas M, Hillenkamp F. Matrix assisted laser desorption/ionization mass spectrometry of enzymatically synthesized RNA up to 150 kDa. *Nucleic Acids Res.* 1994; **22**: 3866–3870.
9. Thiede B, von Janta-Lipinski M. Noncovalent RNA-peptide complexes detected by matrix-assisted laser desorption/ionization mass spectrometry. *Rapid Commun. Mass Spectrom.* 1998; **12**: 1889–1894.
10. Sugaya M, Nishino N, Katoh A, Harada K. Amino acid requirements for the high affinity binding of a selected arginine-rich peptide with the HIV Rev-response element RNA. *J. Pept. Sci.* 2008 (in press).
11. Tan R, Frankel AD. Structural variety of arginine-rich RNA-binding peptides. *Proc. Natl. Acad. Sci. U.S.A.* 1995; **92**: 5282–5286.
12. Beavis RC. Matrix-assisted ultraviolet laser desorption: evolution and principles. *Org. Mass Spectrom.* 1992; **27**: 653–659.
13. Tang K, Allman SL, Chen CH. Matrix-assisted laser desorption ionization of oligonucleotides with various matrices. *Rapid Commun. Mass Spectrom.* 1993; **7**: 943–948.
14. Franklin NC. Clustered arginine residues of bacteriophage λ N protein are essential to antitermination of transcription, but their locale cannot compensate for *boxB* loop defects. *J. Mol. Biol.* 1993; **231**: 343–360.

Journal of Peptide Science
J. Pept. Sci. (2008)
Published online in Wiley InterScience (www.interscience.wiley.com). DOI: 10.1002/psc.1027

JOURNAL OF PEPTIDE SCIENCE

Amino acid requirement for the high affinity binding of a selected arginine-rich peptide with the HIV Rev-response element RNA

MAKI SUGAYA,[a] NORIKAZU NISHINO,[b] AKIRA KATOH[a] and KAZUO HARADA[c]*

[a] Department of Materials and Life Science, Faculty of Science and Technology, Seikei University, Musashino, Tokyo 180-8633, Japan
[b] Graduate School of Life Science and Systems Engineering, Kyushu Institute of Technology, Wakamatsu, Kitakyushu 808-0196, Japan
[c] Department of Life Sciences, Tokyo Gakugei University, Koganei, Tokyo 184-8501, Japan

Received 17 December 2007; Revised 26 January 2008; Accepted 1 February 2008

Abstract: The arginine-rich motif is a class of short arginine-rich peptides that bind to specific RNA structures that has been found to be a versatile framework for the design and selection of RNA-binding peptides. We previously identified novel peptides that bind to the Rev-response element (RRE) RNA of the HIV from an arginine-rich polypeptide library (ARPL) consisting of a polyarginine (15 mer) randomized at the *N*-terminal 10 positions. The selected peptides bound more strongly to the RRE than the natural binding partner, Rev, and contained glutamine residues that were assumed to be important for recognition of the G–A base pair. In addition, the peptides were predicted to bind to the RRE in an α-helical conformation. In this study, in order to understand the mechanism of the interaction between the RRE and the putative α-helical glutamine-containing peptides, the amino acid requirements for high affinity binding were analyzed by a combinatorial approach using a bacterial system for detecting RNA–peptide interactions. A consensus peptide, the DLA peptide, was elucidated, which consists of a single glutamine residue within a polyarginine context with the glutamine residue flanked at specific positions by three nonarginine residues, two of which appear to be important for α-helix stabilization. In addition, the DLA peptide was found to bind extremely tightly to the RRE with an affinity 50-fold higher than that of the Rev peptide as determined by a gel shift assay. A working model for the interaction of the DLA peptide to the RRE is proposed, which should aid in the development of peptide-based drugs that inhibit HIV replication, as well as in our understanding of polypeptide–RNA interactions. Copyright © 2008 European Peptide Society and John Wiley & Sons, Ltd.

Supplementary electronic material for this paper is available in Wiley InterScience at http://www.interscience.wiley.com/jpages/1075-2617/suppmat/

Keywords: HIV RRE RNA; arginine-rich peptide; combinatorial analysis; antitermination system; anti-HIV drugs

INTRODUCTION

RNA–protein interactions play important roles in gene regulation and in the assembly of functional RNA–protein complexes such as the ribosome. Complexes between arginine-rich peptides and their RNA sites have been useful model systems in increasing our understanding of RNA–protein interactions [1–4]. Arginine-rich peptides have been shown to bind to their respective RNAs in a variety of conformations such as an α-helix in the case of HIV Rev and phage N peptides [5–8], a β-hairpin structure in the case of the bovine immunodeficiency virus (BIV) Tat peptide [9,10], and an extended conformation in the case of the HIV Tat peptide [11,12]. The RNA sites to which these peptides bind have been shown to be located at bulged and looped regions within relatively structured RNAs [7,8,13–15], where the narrow major groove of the RNA double helix is widened [16]. Adaptive binding involving unstructured to structured transitions of peptide and/or RNA upon complex formation has also been found to be a general feature [1,17].

The Rev peptide, a short peptide corresponding to the RNA-binding domain of the HIV Rev protein, has been shown to bind to an RNA structure within the HIV genome referred to as the Rev-response element (RRE) (Figure 1). Mutagenesis and chemical modification experiment showed that the Rev peptide binds to an internal loop region of the RRE consisting of G46 to C51 and U66 to C745 of the RRE (Figure 1(A)) [14,18,19]. *In vitro* selection experiments suggested the presence of a noncanonical G48–G71 base pair in the internal loop that can be replaced by an isostructural A48–A71 base pair (Figure 1(A)) [20,21]. The NMR structure of the Rev–RRE complex later confirmed the formation of the G48–G71 base pair as well as a G47–A73 base pair that results in the widening of an otherwise narrow major groove, allowing the binding of the α-helical Rev peptide deep into the RNA major groove [6]. Four specific amino acid side chain–nucleotide base interactions, an asparagine amide group (N40) binding to the G47–A73, the arginine guanidinium groups of R35, R39, and R44 binding

* Correspondence to: Kazuo Harada, Department of Life Sciences, Tokyo Gakugei University, Nukuikita-machi 4-1-1, Koganei, Tokyo 184-8501, Japan; e-mail: harada@u-gakugei.ac.jp

to G67, G70, and U45, respectively, along with several arginine guanidinium–phosphate interactions, and a number of hydrophobic interactions were observed [6].

A number of novel RRE-binding peptides have been identified from random peptide libraries, showing that multiple strategies exist for the recognition of the same RNA site [22–25]. In one such selection experiment using a bacterial reporter assay for detecting RNA–polypeptide interactions, RRE-binding peptides were selected from a randomized library consisting of three amino acids (R, S, and G), then further evolved by mutagenesis and reselection, resulting in the identification RSG-1.2 peptide, which bound to the RRE several times more strongly and specifically than the Rev peptide (Figure 1(B)) [22,23]. Strikingly, while the helical Rev peptide bound along the major groove of the RRE in a manner similar to the binding of α-helices to the major groove of double-stranded DNA [6], the RSG-1.2 peptide was found to bind to a similar region of the RRE in an unstructured-turn-helix conformation with the helix axis of the peptide almost perpendicular to that of the RRE [26,27]. The details of the two interaction have been found to be considerably different, as determined by selection of RRE-variants that bind to RSG-1.2, and comparison of the resulting sequences [28].

In another selection of RRE-binders from a Rev-based library, where the six amino acids important for RRE-binding (Figure 1(B), amino acids in bold) were completely randomized, peptides with a conserved glutamine residue at a position corresponding to the critical asparagine of Rev were identified using a mammalian screening system [24]. The RRE-binding affinity of the glutamine-containing peptides correlated with the α-helical propensity of the peptides, strongly suggesting that this class of peptides binds to the

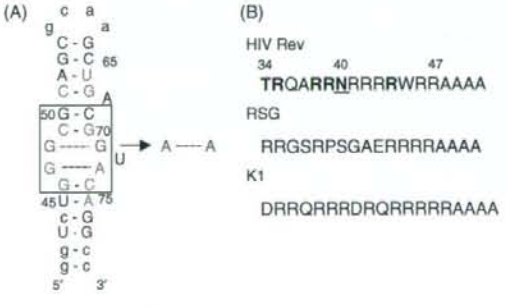

Figure 1 HIV RRE and selected RRE-binding peptides. (A) The secondary structure of the RRE with nucleotides important for Rev-binding shown in red, and those important for RSG-binding boxed. The G–G base pair that may covary to an isostructural A–A base pair, and which is important for K1 binding is shown in blue. (B) Amino acid sequences of Rev peptide and selected peptides, RSG-1.2 and K1. Amino acids within the Rev peptide important for RRE binding are indicated in bold, and the critical asparagine residue that contacts the G–A base pair is underlined.

RRE in a manner similar to the Rev peptide. It was therefore concluded that the critical glutamine binds to the G47–A73 base pair of RRE in a manner analogous to the asparagine residue of the Rev peptide [24]. Strikingly, substitution of the glutamine residue to an asparagine led to loss of binding, as did substitution of the asparagine residue to a glutamine residue in the Rev context.

In an attempt to further identify novel RRE-binders, selection from a complex arginine-rich peptide library, arginine-rich peptide library 1 (ARPL1), which consisted of a 15 mer polyarginine mutagenized at the *N*-terminal 10 positions using 12 nonhydrophobic amino acids at a rate of 50% was carried out using the bacterial screening system mentioned above [25]. As a result, peptides with activities considerably higher than the natural binding partner Rev, and which contained a conserved glutamine residue at a position similar to the glutamine-containing peptides in the above-mentioned selection were obtained [24].

While these results suggested that the glutamine-containing peptides were binding to the RRE in a manner similar to the Rev peptide, the nucleotide base requirements for RRE binding to the Rev peptide and a glutamine-containing peptide, K1, were found to be somewhat different [29]. In particular, the replacement of the characteristic G–G base pair to the isostructural A–A base pair, which is tolerated in the case of the Rev and RSG-1.2 peptide, lead to a loss of binding in the case of the K1 peptide, suggesting that the G–G base pair was being recognized by the K1 peptide.

In this study, in order to understand the mechanism for the high affinity binding of the glutamine-containing arginine-rich peptides with the RRE, combinatorial analysis of amino acids important for binding was carried out. First, in order to understand the sequence variability in all 15 residues of the peptide and possibly identify even stronger binders, two new ARPLs ARPL2 and ARPL3, where all 15 residues were randomized were constructed, and RRE-binding peptides were identified using the bacterial screening system (Figure 2). Comparison of RRE-binding peptides from the two libraries ARPL2 and ARPL3 resulted in the determination of a consensus RRE-binding sequence where the critical glutamine is flanked at a number of specific positions by nonarginine residues within a polyarginine framework. In order to determine the role of the nonarginine positions, a new library, Q3L, was designed to exhaustively screen for optimal amino acids in these positions, resulting in the identification of a consensus RRE-binding peptide, the DLA peptide. The importance of the remaining arginine residues was also determined by alanine- and lysine-scanning experiments. On the basis of these results, a model for the binding of the DLA peptide to the RRE is proposed, and the basis for the high affinity RRE-binding by the DLA peptide is discussed.

DOI: 10.1002/psc

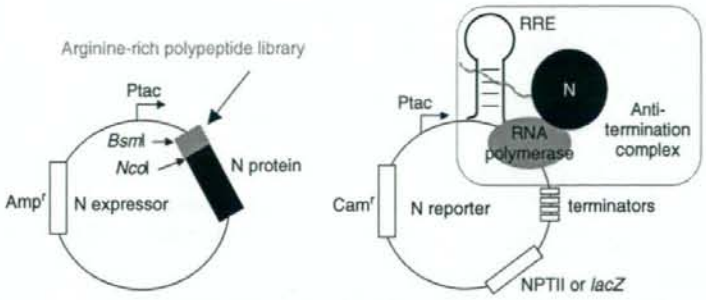

Figure 2 The two-plasmid system for detecting RNA–polypeptide interactions by λ N-mediated transcriptional antitermination. The arginine-rich polypeptide libraries ARPL2 and ARPL3 were fused to the N protein and expressed under the control of a tac promoter from a pBR322-based plasmid (N expressor). The pACYC-based reporter plasmid (N reporter) contains the *LacZ* gene or *NPT II* gene, also under the control of the tac promoter, so that binding of library peptides to the RRE results in reporter gene expression.

RESULTS

Selection of RRE-binding Peptides from the ARPL2 and ARPL3 Libraries

The glutamine-containing peptides identified in the previous study were identified from the ARPL1 library, which was randomized at the first 10 positions within a 15 mer polyarginine framework [25]. In order to determine those positions within the 15 residue peptide that are important for RRE-binding, two new libraries, ARPL2 and ARPL3, that were mutagenized at all 15 arginine residues at the codon level using 12 nonhydrophobic amino acids were constructed [30] and RRE-binding peptides were identified using a bacterial two-plasmid system (Figure 2) [22,25]. The doped polyarginine library was flanked at the *N*-terminus by two randomized amino acids; at the *C*-terminus by alanine residues, which stabilize α-helices in the case of ARPL2, and glycine residues, which destabilize α-helices in the case of ARPL3 (Figure 3).

Both selections were carried out using a four-step procedure to enrich RRE-binding sequences while eliminating reporter-related false positives and nonspecific positives [25]. In the first round, library plasmids encoding the ARPL2 and ARPL3 libraries were transformed into RRE-reporter cells carrying the kanamycin resistance reporter to yield 3.7×10^7 and 1.1×10^8 total transformants on plates containing 5 μg/ml of kanamycin, of which a total of 1.1×10^5 (0.29%) and 3.1×10^5 colonies (0.3%) survived, respectively. In the second round, pooled library plasmid DNA from each of the two first round survivors was then transformed into RRE-reporter cells, and the cells were spread on plates containing 10 μg/ml kanamycin to further enrich for tight binders and to reduce the background from reporter-related

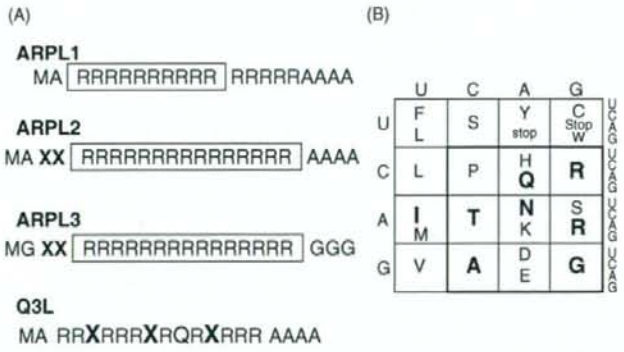

Figure 3 (A) Arginine-rich peptide libraries (ARPLs) used in this study. The doped regions of ARPLs are boxed. ARPL1 consisted of a polyarginine (15 mer) codon-mutagenized at 10 positions using 12 nonhydrophobic amino acids at a rate of 50% [25,29]. ARPL2 consisted of a 15 mer polyarginine codon-mutagenized at all 15 positions using 12 nonhydrophobic amino acids at a rate of 50%, and an additional 2 randomized amino acids at the *N*-terminal, indicated by X. ARPL3 consisted of the same doped region as ARPL2, but was flanked by glycines instead of alanines. Q3L consisted of a polyarginine (14 mer) mutagenized at 3 positions using 20 amino acids and a glutamine at position 9. (B) The genetic code viewed from the perspective of arginine rich peptides. The 12 amino acids used in the libraries are encoded by 18 codons, as indicated by the boldfaced box in the codon chart.

false positives. Of the $\sim 3.6 \times 10^7$ total transformants for the ARPL2 selection and the $\sim 5.6 \times 10^7$ total transformants for the ARPL3 selection, 1.1×10^6 (3.1%) and 5.1×10^5 (0.9%) colonies survived, respectively. In the third round, pooled plasmid DNA from each of the second round survivors was transformed into pAC-RRE reporter cells carrying the *lacZ* reporter and the cells were plated onto X-gal plates. In the case of the ARPL2 selection, 99% of colonies that survived two rounds of kanamycin selection were blue, while in the case of the ARPL3 selection only 51% of colonies that survived two rounds of kanamycin selection were blue. In the fourth round, plasmid DNA from 28 of the darkest blue colonies in each selection were individually tested against the RRE reporter and the BIV TAR reporter. All clones showed β-galactosidase expression in with the RRE reporter and not with the BIV TAR reporter. In the ARPL2 selection, sequencing of the 28 clones resulted in the identification of 11 unique clones encoding peptides that contained a glutamine residue at either the 9th or 10th position of the polyarginine stretch, similar to RRE-binders from the ARPL1 [25], were identified (Table 1). In the case of the ARPL3 selection, six unique clones encoding peptides that contained a glutamine residue at either the 9th or 10th position of the polyarginine stretch, similar to RRE-binders from the ARPL1 and ARPL2 libraries [25], were identified (Table 1).

Analysis of RRE-binding Peptides Identified from ARPL1~3 Libraries, and Reselection from the Q3L Library

Upon alignment of RRE-binding peptides obtained from ARPL2 and ARPL3 selections at the glutamine residue, while the majority of positions appeared to require arginine residues for binding, three positions −6, −2, and +2 relative to glutamine contained aspartic acid, glutamic acid, and alanine residues at high frequencies (Table 1). Since the selected peptides were predicted to bind to the RRE in an α-helical conformation based on the similarity to the glutamine-containing peptides obtained in a previous selection [24], axial views of the putative α-helical peptides are shown in Figure 4. As

Table 1 RRE-binding peptides selected from ARPL2 and ARPL3

	Clone No.			Peptide sequences[a]		Antitermination activity (X-gal[b])	
						HIV RRE	(BIV TAR)
ARPL2							
Class I[c]	2-17	MA	SA	RRRRRRRRR**Q**RARRR	AAAA	7.5	0
	2-28	MA	SD	PRR**Q**RRRRR**Q**RARRR	AAAA	6	0
Class II[c]	2-07	MA	NP	ARRARRRCR**Q**RERRR	AAAA	7	0
	2-11	MA	SL	RRNRRRSR**Q**RARRRE	AAAA	6	0
	2-06	MA	IL	ARR**Q**RRRGR**Q**RERRR	AAAA	6	0
Class III[c]	2-42	MA	ND	RRRRRRTR**Q**RDRRRN	AAAA	6.5	0
	2-04	MA	QR	ERRERRRER**Q**RNRRK	AAAA	6.5	0
	2-09	MA	YA	DRRKRRRER**Q**RRRRA	AAAA	5	0
	2-26	MA	LL	PRRERRRRR**Q**RERRR	AAAA	6	0
	2-39	MA	SR	DRTRRRRTR**Q**RSRRR	AAAA	6.5	0
	2-08	MA	VA	TRRERRRRR**Q**RTRRR	AAAA	5	0
ARPL3							
Class I[c]	3-07	MG	AN	ARRRRRRAR**Q**RARRR	GGG	6	0
	3-13	MG	DT	RRRRRHAR**Q**RERRRR	GGG	5	0
Class II[c]	3-14	MG	LS	PRRDKRRRR**Q**RARRR	GGG	5	0
Class III[c]	3-01	MG	PH	RR**Q**RRRDR**Q**RRRRRA	AAA	6	0
	3-04	MG	LE	RRRRRRRDR**Q**RKRRS	GGG	5	0
	3-12	MG	LL	RRDRRR**Q**R**Q**R**Q**RRRR	GGG	6	0
Rev				TR**Q**ARRNRRRRWRR		3	0
RSG-1.2				RDRRRRGSRPSGAERRRR		4	0
K1		MA		DRR**Q**RRRDR**Q**RRRRR	AAAA	6	0
BIV Tat				MSGPRPRGTRGKGRRIRR		0	3

[a] The conserved glutamine residue is shown in bold, and the nonarginine residues are underlined.
[b] The number of plusses indicates blue color scored by the colony color (X-gal) assays that were performed as described [25].
[c] Selected peptides were classified into three groups based on the types of amino acids observed in the nonarginine positions. Class I peptides contained mostly hydrophobic amino acids. Class II peptides contained both hydrophobic amino acids and acidic amino acids. Class III peptides contained mostly acidic amino acids.

DOI: 10.1002/psc

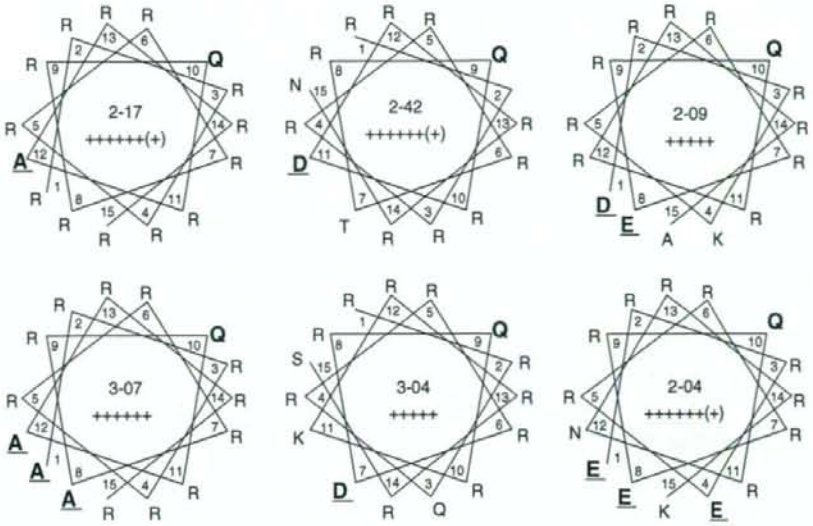

Figure 4 Axial view of the putative α-helical conformations of representative RRE-binding peptides. The nonarginine residues (alanines and acidic amino acids) are underlined, and the critical glutamine (Q) residue is shown in bold. The number of plusses indicates blue color scored by the colony color (X-gal) assay.

a result, the three nonarginine residues are positioned opposite to the conserved glutamine residue. In order to determine the role of amino acids at the three nonarginine positions and to identify the peptides that bind more strongly to the RRE, a new library, Q3L, was designed. The Q3L library consisted of 14 mer polyarginines with the glutamine residue important for RRE-binding at the 9th position, and positions −6, −2, and +2 relative to the glutamine completely randomized with 32 codons encoding the 20 amino acids, and resulting in a total of $32^3 = 32\,768$ codon sequences (Figure 3(A)).

In the case of the Q3L library, RRE-binding peptides were screened using RRE-LacZ reporter cells. In the first round, $\sim 6.6 \times 10^5$ colonies were screened, and 20% of the colonies were blue. Of these blue colonies, 1248 colonies with varying blue intensity were pooled, and pBR library plasmid DNA was isolated. In the second round, this library plasmid was retransformed into RRE-reporter cells, and 72% of colonies were blue. Plasmids were isolated from 70 clones of varying blue intensity, and scored as 2+ ~ 6+, relative to the Rev peptide (3+) and RSG-1.2 peptide (4+). Of these 70 clones, 59 were found to be unique sequences. The sequence of the clones exhibiting blue intensities of 6+, 5+, 4+, 3+, and 2+ are shown in Supplementary Table 1, and the relationship between antitermination activity and amino acid identity at the three positions is shown in Figure 5. At position −6 relative to glutamine, clones with high antitermination activities had a preference for acidic amino acids, in particular, aspartic acid (D) (Figure 5(A), Supplementary Table 1). At position −2 and +2, clones with high antitermination activities both had a preference for aliphatic amino acids, in particular, leucine (L) and alanine (A), respectively (Figure 5(B) and (C), Supplementary Table 1). This tendency diminished at each position as the intensity of blue decreased, and in the case of 3+ and 2+ clones, no clear preference could be observed (Figure 5(A–C)). On the basis of these results, the DLA peptide, which contains an asparagine (D) at position −6, a leucine (L) at position −2, and an alanine (A) at position +2, was chosen as the optimal sequence for RRE binding.

In order to confirm the importance of these positions for RRE-binding, three mutant DLA peptides that were expected to show decreased activity, with a D to R substitution at position −6 (RLA peptide), an L to N substitution at position −2 (DNA peptide), and an A to E substitution at position +2 (DLE peptide), as well as a peptide where all three positions were substituted by arginines (R8QR5) were tested *in vivo* using the antitermination assay. As a result, all three peptides with single amino acid substitutions showed blue color intensities of 3.5+ ~ 4+, and substitution of all three positions led to a complete loss of activity (Table 2). On the other hand, a peptide with a substitution of the conserved glutamine to an asparagine residue (Table 2, DLA Q9N) did not show activity, as in the case of a previously reported RRE-binding peptide containing glutamine [24]. Gel shift analysis of the affinity of RRE-binding by the DLA peptide and the three mutant peptides RLA, DNA, and DLE showed that the activities reported *in vivo* reflect the strength of RNA-peptide